RSC Advances

REVIEW

View Article Online
View Journal | View Issue



Cite this: *RSC Adv.*, 2025, **15**, 17843

# A review of the developments in adsorbents for the efficient adsorption of ibuprofen from wastewater

Ahmer Ali Siyal, *[a] Radin Maya Saphira Radin Mohamed, *[ab] Faizan Ahmad, [c] Marlinda Abdul Malek, [d] Majed Alsubih, [e] Rashid Shamsuddin, [f] Sajid Hussain[g] and Sabariah Musa [b]

This paper critically evaluates the recent advancements in developing adsorbents to remove ibuprofen (IBU) from wastewater. Adsorbent characteristics, their performance in removing IBU from wastewater in batch and column studies, the adsorption kinetics, isotherms, thermodynamics, and mechanisms, adsorbent regeneration, continuous adsorption, and future challenges are included in this paper. Activated carbons, nanomaterials, metal–organic frameworks, biochar, and other adsorbents have been developed to remove IBU from wastewater. Most adsorbents were mesoporous, while some were macro- and microporous, and they contained acidic and basic functional groups. Adsorbents' surface areas range from 2.38 to 2900 $m^2\ g^{-1}$, pore sizes from 0.0195 to 87.3 nm, and pore volumes from 0.006 to 14.48 $cm^3\ g^{-1}$. The adsorption capacity ranged between 0.220 mg $g^{-1}$ to 497.3 mg $g^{-1}$, with Cu-doped Mil-101(Fe) and *Albizia lebbeck* seed pods activated carbon (MSAC) adsorbents achieving the highest and lowest adsorption capacities. The optimal pH of 2–8, dose of 0.012–10 g $L^{-1}$, IBU concentration of 0.07–200 mg $L^{-1}$, and the equilibrium time of 0.083–120 h were obtained. The pseudo-second order and Langmuir isotherm models generally fit the data, showing that IBU was adsorbed through the chemisorption process by producing a monolayer of IBU onto the adsorbent, and the thermodynamics described the adsorption of IBU as a spontaneous and endothermic or exothermic process. The IBU was adsorbed through various mechanisms such as electrostatic interactions, π–π interactions, pore filling, pore diffusion, π–π EDA interactions, hydrogen bonding, and Yoshida interactions. More focus should be put on developing highly efficient, economical, green, and regenerable adsorbents that can adsorb multiple drugs from wastewater. Mass transfer adsorption kinetics should be studied to better understand adsorption processes, and artificial intelligence technologies should be utilized in IBU removal from wastewater to anticipate the adsorption capacity of adsorbents. This review serves as a guide in enhancing the performance of adsorbents in removing pharmaceuticals from wastewater.

Received 22nd March 2025
Accepted 22nd May 2025

DOI: 10.1039/d5ra02007g

rsc.li/rsc-advances



## 1. Introduction

The condition of water resources is deteriorating, as almost 4000 emerging micropollutants (MPs) have been detected in surface waters.[1] MPs such as pharmaceuticals, fluorinated surfactants, and personal care products (PCPs) have been detected in wastewater. The main sources of MPs are households, agriculture, industries, and transport activities.[2] Pharmaceuticals contribute to the contamination of water resources, as many of these chemicals cannot be absorbed by humans and are released into the wastewater.[3] They enter water resources by throwing unused and expired pharmaceuticals into the drainage system and through the excretion of humans and animals.[4] The presence of pharmaceuticals in wastewater treatment plant (WWTP) effluents suggests that these substances cannot be eliminated from wastewater by the current WWTPs.[5] Pharmaceuticals reach humans through the food chain by consuming foods obtained from contaminated water resources (Fig. 1).

About 32 drugs have been found in German WWTPs. The highest levels of ibuprofen (IBU) were found in the sewage (3.4 μg $L^{-1}$) and the river stream (0.53 μg $L^{-1}$).[6] In Portugal, the pharmaceuticals were higher in hospital wastewater, ranging

[a]*Micropollutant Research Centre (MPRC), Institute for Integrated Engineering (I²E), Universiti Tun Hussein Onn Malaysia, 86400 Parit Raja, Batu Pahat, Johor, Malaysia. E-mail: maya@uthm.edu.my*

[b]*Faculty of Civil Engineering and Built Environment, Universiti Tun Hussein Onn Malaysia, 86400 Parit Raja, Batu Pahat, Johor, Malaysia*

[c]*School of Computing, Engineering and Digital Technologies, Teesside University, Middlesbrough, UK*

[d]*Water and Environmental Engineering Department, Faculty of Civil Engineering, Universiti Teknologi Malaysia, 81310, Johor, Malaysia*

[e]*Department of Civil Engineering, King Khalid University, Abha, Saudi Arabia*

[f]*Department of Chemical Engineering, Faculty of Engineering, Islamic University of Madinah, 42311 Madinah, Saudi Arabia*

[g]*Department of Civil, Environmental, and Mechanical Engineering, University of Trento, ViaMesiano 77, Trento, Italy*

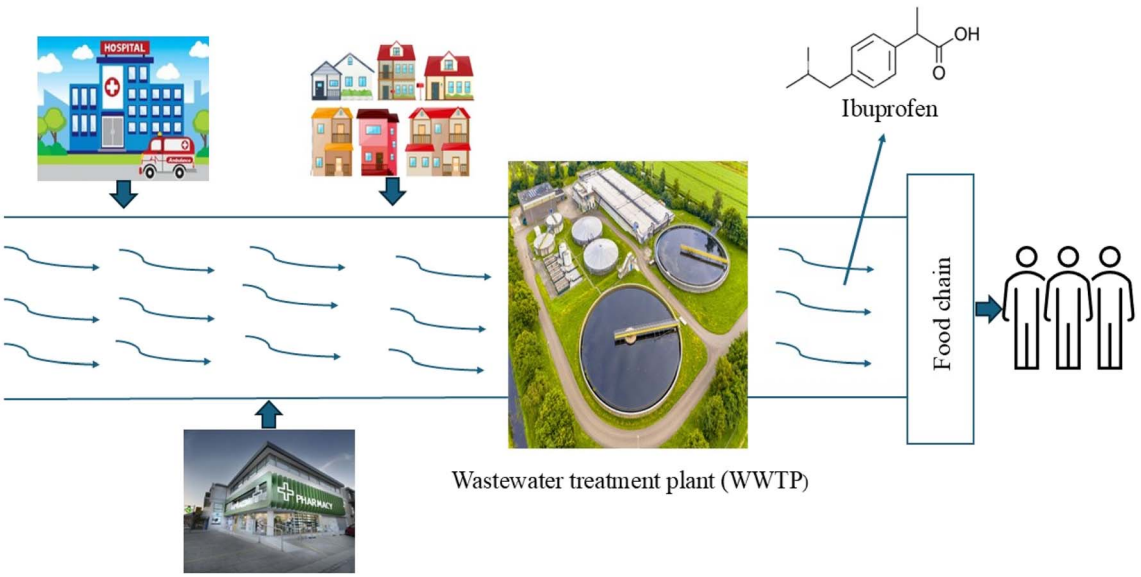


Fig. 1 Sources of discharge of pharmaceuticals and contamination of water sources.

from 5.82 μg $L^{-1}$ to 38.15 μg $L^{-1}$ depending on the type of hospital (university hospital, general hospital, maternity hospital, and pediatric hospital), but the effluents after treatment contained a maximum IBU concentration of 0.37 μg $L^{-1}$.[7] In Norway and Italy, IBU in hospital wastewater was 8.96 μg $L^{-1}$ and 3.20 μg $L^{-1}$.[8,9] The IBU in groundwater was around 3 to 395 ng $L^{-1}$ in Europe in 2014.[10] Pharmaceutical substances affect aquatic creatures in various ways, including changing their behavior, upsetting their hormonal balance, and reducing their reproduction ability.[11,12] Some drugs can also disturb the growth of algae and other aquatic plants, potentially affecting the food chain.[13] They also cause aquatic toxicity and produce antibiotic-resistant bacteria.[14]

IBU is a non-steroidal anti-inflammatory drug that relieves pain and fever.[15] It's extensively utilized globally, with annual production rates of approximately 200 tons.[16] It is commonly detected in wastewater due to usage in large quantities and incomplete removal by wastewater treatment systems.[17] Its chemical name is 2-(4-isobutylphenyl)propanoic acid, which has an acid–base constant or dissociation constant ($pK_a$) of 4.91, showing that it is a weak acid with a low adsorption tendency on wastewater treatment sludge[18] (Table 1). The carboxyl group in IBU makes it ionizable and present in an anionic form when its pH is above $pK_a$, and in a neutral form if pH is below its $pK_a$. Electrostatic interactions depend on the charges on the adsorbent and IBU, while the carboxyl group in IBU acts as a hydrogen bond donor and hydrogen bond acceptor during the hydrogen bonding of IBU onto the adsorbent. The phenyl rings in the structure of IBU are responsible for pi–stacking interactions with aromatic rings if available on the adsorbent. It has the main functional groups of benzene and carboxylic acids, which make it more movable and less soluble in water.[19] The lower solubility of IBU in water, high lipophilicity ($\log K_{ow}$), and low adsorption coefficient ($\log K_{oc}$) show that it has low mobility and no adsorption tendency in the soil.[20] The $\log K_{ow}$ is a physicochemical parameter inversely proportional to the compound's solubility. The compounds with $\log K_{ow}$ above 4 are hydrophobic, and those with $\log K_{ow}$ below 2.5 are considered low hydrophobic. Hydrophobicity is directly proportional to adsorption. IBU can be found in wastewater in its original form or as hydroxyl-IBU or carboxyl-IBU metabolites[1] (Fig. 2). It has been noticed that the adsorbents with acidic surface properties possess a higher affinity for relatively hydrophilic IBU sodium

Table 1 Properties of ibuprofen

| | |
|---|---|
| Molecular formula | $C_{13}H_{18}O_2$ |
| $pK_a$ (acid–base constant) | 4.91 |
| $\log K_{ow}$ ($K_{ow-octanol}$ water coefficient) | 3.97 |
| $\log K_{oc}$ ($K_{oc}$ adsorption coefficient) | 2.5 |
| Molar mass | 206.29 g $mol^{-1}$ |
| Density | 1.03 $cm^3$ $g^{-1}$ |
| Solubility in water | 0.021 mg $cm^{-3}$ (20 °C) |
| Specific gravity | 1.03 |
| Boiling point | 157 °C |
| Melting point | 75–78 °C |
| Molecular dimensions | 0.43–1.03 nm |

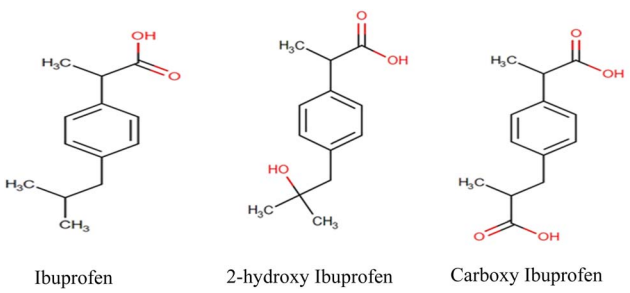


Fig. 2 Chemical structure of ibuprofen and its metabolites in wastewater.

salt molecules than more basic adsorbents.[18] Although IBU is present in low concentrations in drinking water, the continuous uptake of IBU-contaminated water can seriously impact human health.[21] The IBU in drinking water deteriorates the taste and odor of water and decreases its appeal to consumers. It severely damages the liver and kidneys and causes gastrointestinal issues.[22]

Various techniques, such as membranes, advanced oxidation processes (AOPs), and hybrid methods, are used for removing IBU from wastewater. These techniques are difficult, require significant maintenance costs, and generate more waste. Adsorption is a preferred method due to its efficiency, simplicity, and environmental friendliness.[23] Various adsorbents such as activated carbons, nanomaterials, Metal–Organic Framework (MOF), biochar, and others have been used to remove IBU from wastewater. Several reviews have been published on IBU removal from wastewater. Chopra and Kumar[22] published a review paper on the IBU removal methods from wastewater. Show *et al.*[24] conducted a comprehensive review on eliminating IBU from wastewater, specifically emphasizing adsorption and bioremediation. Oba *et al.*[25] wrote a review paper about how to adsorb IBU from wastewater, focusing on how well different adsorbents developed during 2010–2020 removed IBU. Ahmed[26] published a review paper discussing the elimination of IBU and carbamazepine from water using adsorbents derived from agricultural waste. Wu *et al.*[27] published a review paper on IBU and acetaminophen removal from municipal wastewater treatment plants. Ayati *et al.*[28] reviewed the adsorption of IBU using porous carbonaceous materials. Segovia *et al.*[29] conducted a bibliometric statistical analysis on eliminating triclosan, ibuprofen, amoxicillin, and paracetamol utilizing organic residues. Different organic residues, such as activated carbons, shells, and husks, were studied. No review paper on recent advancements in adsorbent development for IBU removal from wastewater has recently been published.

This paper critically reviews the performance of recently developed adsorbents in removing IBU from wastewater. It includes the characteristics and performance of adsorbents in batch studies, the adsorption kinetics, isotherms, thermodynamics, mechanism, and regeneration of adsorbents. The adsorbent's performance in continuous studies and the future challenges in IBU adsorption are also discussed.

## 2. Adsorption of ibuprofen

### 2.1 Batch adsorption

**2.1.1 Activated carbons.** The activated carbons possess high surface areas (500–3000 $m^2\ g^{-1}$), good micropore volume, and high charge holding capacity.[30] They are expensive materials due to the high temperatures required during their synthesis. Various activated carbons derived from diverse sources have removed IBU from wastewater. The *Nauclea diderrichii* biomass-derived activated carbon (NDAC) adsorbent at 298 K obtained a $q_m$ of 56.82 mg $g^{-1}$. The functional groups of C=C and C=O were mainly involved in the adsorption of IBU, and the adsorption capacity increased due to an increase in the mesoporosity of the adsorbent.[31] This work developed a good adsorbent for IBU removal from wastewater; however, its IBU adsorption performance is lower than most other adsorbents used to remove IBU. Modifying its surface with appropriate materials to enhance its surface area and active adsorption sites can enhance its performance. Two activated carbons prepared from cork waste by chemical activation with $K_2CO_3$ (CAC) and chemical activation with $K_2CO_3$ and steam activation (CPAC) showed changes in their point of zero charge (PZC) due to the changes in the surface chemistry. CAC had a more acidic surface (PZC-7.5) than CPAC (PZC-9.9), which was due to the presence of higher oxygen functional groups on CAC compared to CPAC. Steam activation decreased the contents of R-OH and removed R-COOH and R-OCO functional groups and increased the R=O functional groups in CPAC. The CAC and CPAC achieved the $q_m$ of 139.2 mg $g^{-1}$ and 393.4 mg $g^{-1}$, respectively, at ambient temperature. The higher adsorption affinity of CPAC was due to its highly developed super microporous structure, which makes it a viable and economical adsorbent for removing IBU from wastewater.[19] Two adsorbents of beverage sludge-activated carbon (BSAC) and acid-treated beverage sludge-activated carbon (ABSAC) showed that ABSAC contained smaller particles and more surface roughness as compared to BSAC, which was due to the leaching of impurities during acid treatment, as shown in Fig. 3. The microstructure of BSAC (Fig. 3(a and b)) is disorganized, having low roughness and low porosity due to the presence of impurities in the material. The microstructure of ABSAC (Fig. 3(c and d)) is more organized and shows small particles with higher roughness and higher porosity due to the removal of impurities. It helped the ABSAC adsorbent to adsorb more IBU molecules than BSAC. The ABSAC obtained a $q_t$ of 105.91 mg $g^{-1}$ at the best parameters of pH 4, room temperature, and equilibrium time of 180 min. The ABSAC was also tested on pharmaceutical effluent containing ibuprofen, ketoprofen, and paracetamol, and it removed 85.16% of pharmaceuticals.[32] This study developed an efficient and sustainable adsorbent from waste material, and the increase in adsorption capacity compared to its raw form was associated with the increase in porosity, roughness, and the presence of small particles. Six activated carbons prepared from red mombin seeds (RMS), corn cobs (CC), external sections of mango seeds (MSEP), coffee husk (CH), ice cream bean seeds (GS), and mango seeds internal parts (MSIP) showed differing IBU adsorption performances with RMS, CC, and MSEP adsorbents obtained the $q_t$ of 69.88, 88.03, and 52.60 mg $g^{-1}$, respectively. The rapid rate of graphitization, greater abundance of oxygen groups, and significant micropore volume all contributed to the enhanced adsorption capabilities of the adsorbents. The adsorption of IBU was more advantageous in micropores with pore diameters less than 1.2 nm. The micropore volume of activated carbon adsorbents in the micropore size range of <1.2 nm ranged between 64–74% of the total volume. The micropore volume of these RMS, CC, and MSEP was 73% (0.574 $cm_{liq}^3\ g^{-1}$), 74% (0.494 $cm_{liq}^3\ g^{-1}$), and 69% (0.489 $cm_{liq}^3\ g^{-1}$), respectively.[33] It shows that micropore volume also contributes to enhancing the adsorption capacities of the studied adsorbents. The lower adsorption capacities of

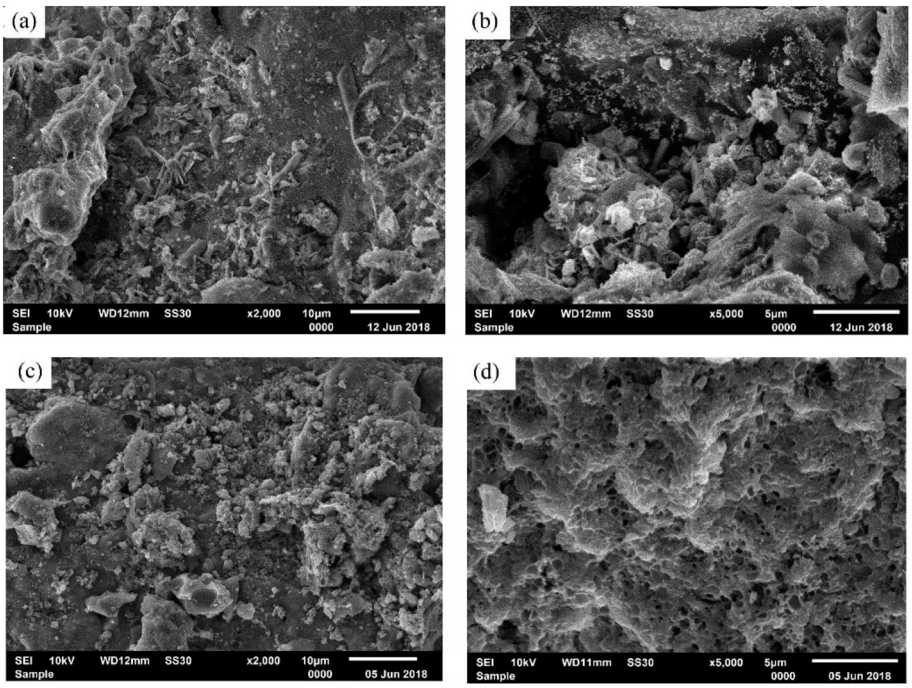


Fig. 3 Microstructure of BSAC (a) and (b) and ABSAC (c) and (d) adsorbents.[32]

CH, GS, and MSIP may also be related to the lower porosity of these adsorbents.

The porous carbon derived from MOF (zeolitic-imidazolate framework-8 (ZIF-8)) (PCDMs) through pyrolysis at 800 °C, 1000 °C, and 1200 °C indicated that the PCDM-1000 having a surface area of 1855 $m^2 g^{-1}$ (Table 3) achieved a $q_m$ of 320 mg $g^{-1}$ that was three times higher than the activated carbon as shown in Fig. 4.[34] The PCDMs showed considerable amounts of acidic (carboxyl, lactone, and phenol) and basic functional groups on the surface of PCDMS. The increase in calcination temperature decreased the amounts of carboxylic and lactone functional groups, while the phenol content decreased in the following order: PCDMS-800 < PCDMS-1200 > PCDMS-1000. The increase in temperature decreased the basic functional groups.[34] This work developed an efficient and recyclable adsorbent with good adsorption capacity, but its adsorption capacity is lower than chemically and steam-activated cork waste (CPAC) and physically activated cork powder. Further enhancement in its performance can be made by improving its surface chemistry by increasing the content of phenolic groups through doping with some suitable materials. Ethylamine-modified hydrophobic activated carbon (HAC-EA) derived from date palm leaflets achieved a $q_t$ of 35.21 mg $g^{-1}$, lower than the original activated carbon. The competition among methanol molecules for hydrophobic sites diminished the adsorption capability of HAC-EA. It achieved higher adsorption in deionized water compared to hospital wastewater. The adsorption capacity decreased in the following order: oxidized activated carbon (OAC) > AC > HAC-EA > ethylene diamine basic surface activated carbon (BAC-EDA), as shown in Fig. 5.[23] The adsorbents' decreasing order of adsorption capacity is similar in both wastewaters. However, the adsorption capacities of adsorbents are higher in deionized water as compared to their adsorption capacities in deionized spiked hospital wastewater, which is due to the presence of dissolved organic substances in spiked hospital wastewater that create competition for active adsorption sites on the adsorbent. The adsorption equilibrium time of adsorbents was in the order of HAC-EA > OAC > BAC-EDA > AC. This work shows that functionalized activated carbon can play a better role in adsorption than unfunctionalized adsorbents. The adsorption performance of HAC-EA needs further improvement by increasing its surface area and active adsorption sites. Two activated carbons prepared from cork waste by chemical activation with $K_2CO_3$ (CAC) and chemical

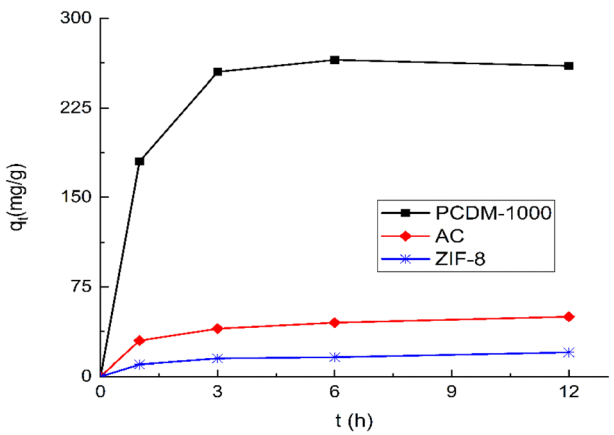


Fig. 4 The adsorption of IBU onto PCDM-1000, AC, and ZIF-8 (redrawn).[34]

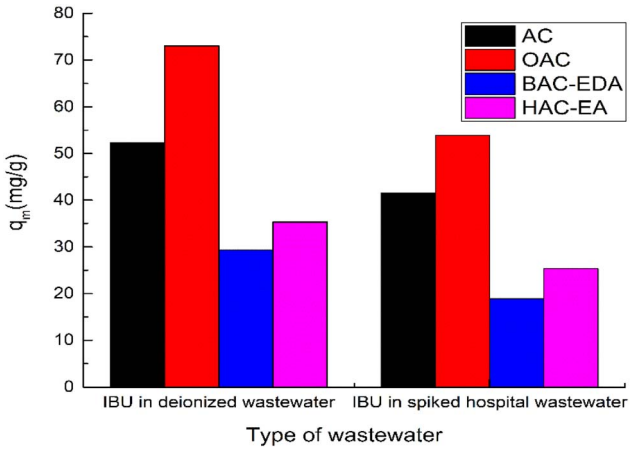


Fig. 5 Adsorption performance of IBU in deionized and spiked HWW (drawn by using data from ref. 23).

activation with $K_2CO_3$ and steam activation (CPAC) showed changes in their point of zero charge (PZC) due to the changes in the surface chemistry. CAC had a more acidic surface (PZC-7.5) than CPAC (PZC-9.9), which was due to the presence of higher oxygen functional groups on CAC compared to CPAC. Steam activation decreased the contents of R-OH and removed R-COOH and R-OCO functional groups, and increased the R═O functional groups in CPAC.[19]

Magnetic nanoparticles incorporated on yeast-based activated carbon (NP-YC) achieved an adsorption capacity of 51 mg $g^{-1}$ from deionized water, which is lower than the adsorption capacity of YC of 107 mg $g^{-1}$. During competitive adsorption with caffeine (CA), NP-YC achieved removal efficiencies above 70% in deionized water and above 60% in primary sewage effluent (PE).[35] This work developed an economical adsorbent using yeast, but its IBU adsorption performance needs further enhancement by improving its surface functionalization with suitable materials. A groundnut shell-activated carbon modified with titanium dioxide nanoparticles ($TiO_2$-NPs-GNSAC) achieved a removal efficiency of 81.78% for IBU from wastewater at optimum conditions, which were optimized using BBD of RSM. Adding $TiO_2$ NPs into activated carbon enhanced its removal performance due to the increased active adsorption sites. The addition of $TiO_2$ NPs into the GNSAC matrix resulted in a reduction in the pore size, pore volume, and surface area of the modified adsorbent ($TiO_2$-NPs-GNSAC).[36] A magnetic composite of nickel-iron oxide nanoparticles and activated carbon ($NiFe_2O_4$/activated carbon-NiAC) obtained a $q_m$ and removal efficiency of 261.35 mg $g^{-1}$ and 86.46% at optimal pH 2, respectively. It achieved a removal efficiency of 86.46% in simulated effluent containing IBU, ketoprofen, and inorganic compounds.[37] Its performance is better than many adsorbents but lower than some adsorbents. The recovery of this adsorbent is very easy using external magnetic force, which reduces the process cost by removing the associated costs of centrifugation and filtration. Carbon nanospheres (CNs) achieved a $q_t$ of 356.899 mg $g^{-1}$ and a removal efficiency of 94.47%, while its removal efficiency decreased to 67% in real wastewater. CNs only showed good adsorption of IBU in synthetic wastewater, while its performance in real wastewater needs further improvement.[38] *Erythrina speciosa* (Ery-AC) showed an amorphous and porous structure with various functional groups, but the C═C functional group was absent, which is involved in π–π interactions during adsorption, and it shows that the IBU will be adsorbed through electrostatic or hydrogen bonds. The Ery-AC obtained a $q_t$ and removal efficiency of 98.11 mg $g^{-1}$ and 65.54% for higher IBU concentration (50–200 mg $L^{-1}$), respectively, and 90% for a lower IBU concentration from a solution containing a mixture of adsorbates. The adsorption of IBU from a simulated effluent containing IBU (50 μg $L^{-1}$), paracetamol (10 μg $L^{-1}$), naproxen (10 μg $L^{-1}$), and ketoprofen (μg $L^{-1}$) showed good removal of IBU with a removal efficiency of 95.2% and higher than 90% for other pharmaceuticals.[39] This work developed an efficient and sustainable adsorbent from seed pods of the forest species *Erythrina speciosa*, but its removal efficiency for higher IBU concentration solution needs further enhancement. Two inexpensive laboratory-developed activated carbons from rice husk (AC-RH) and peach stones (AC-PS) outperformed commercial granular activated carbon (AC-F400) and multiwalled carbon nanotubes (MWCNTs) in adsorbing tetracycline and IBU, with adsorption capacities of 845.9 mg $g^{-1}$ and 239.8 mg $g^{-1}$, respectively.[18] The isoelectric points of AC-RH, AC-PS, AC-F400, and MWCNTs were 3.4, 3, 5, and 6.3, respectively. AC-F400 was 80% microporous, AC-PS was 30% mesoporous, and AR-CH and MWCNTs contained mesopores and macropores.[18] This work developed two efficient and sustainable adsorbents for tetracycline and IBU removal. A nitrogen-doped porous carbon (NPC-2) obtained a $q_m$ of 113 mg $g^{-1}$ in 1 hour of equilibrium time. Higher nitrogen concentration and the adsorbent's microporous and mesoporous structures contributed to the higher adsorption capacity. There was a small effect of the presence of NaCl and humic acid on the adsorption of IBU onto NPC-2. NPC-2 also performed well in removing IBU from lake water (94%, IBU-5 mg $L^{-1}$).[40] Although it can remove IBU from spiked wastewater at low IBU concentrations, the adsorption performance of NPC-2 from real wastewater at higher IBU concentrations would further shed light on its real-world applications. The composite hydrogel beads of alginate-activated carbon and carboxymethyl cellulose (Alg/AC/CMC) displayed good adsorption capacity after reswelling compared to Alg/AC without CMC (34 mg $g^{-1}$ and 18 mg $g^{-1}$ with adsorption capacity before reswelling of 39.6 mg $g^{-1}$). The purpose of adding CMC into the composite hydrogel was to recover its surface area by soaking it in deionized water through a reswelling process. The adsorption capacity and recovery of Alg/AC/CMC after drying were influenced by the activated carbon content and the degree of saturation (DS) of CMC. The wet composite hydrogel beads of Alg/AC/CMC with high water content showed an irregular and rough surface with bumps on the surface, while the dried hydrogel showed a tight structure with disappeared pores due to shrinkage of the structure caused by drying. However, after reswelling with distilled water (DW), the hydrogel recovered to its original morphology, as shown in Fig. 6.[41] This work developed an adsorbent that can be used for

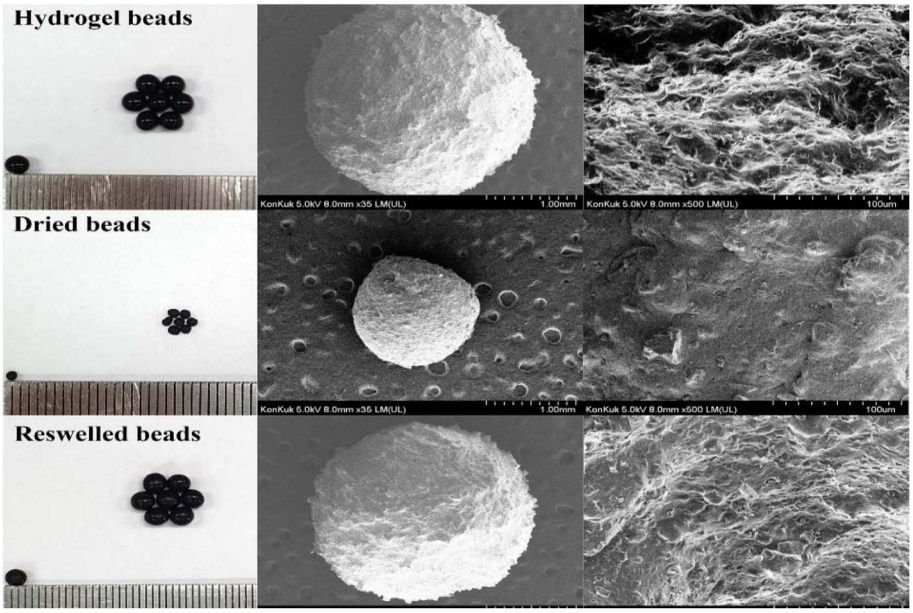


Fig. 6 Morphology of composite beads of Alg/AC/CMC (4%, 1%, 1%).[41]

a longer period by recovering its before-drying properties by soaking it in distilled water.

The surface area, pore size, and pore volume of activated carbons ranged between 4.4 and 1946 $m^2\ g^{-1}$, 1.23 and 16.8 nm, and 0.0017 and 0.80 $cm^3\ g^{-1}$, as shown in Table 3. The adsorption capacities of activated carbons range between 0.220 mg $g^{-1}$ and 356.89 mg $g^{-1}$. Carbon nanospheres (CNs) and *Albizia lebbeck* seed pods activated carbon (MSAC) achieved the highest and lowest adsorption capacities, respectively. The adsorption capacities of carbon nanospheres (CNs), waste coffee-activated carbon (WAC), and nitrogen-doped porous carbon (NPC-2) adsorbents were above 100 mg $g^{-1}$, while all other activated carbon adsorbents' adsorption capacities were below 100 mg $g^{-1}$, as shown in Table 2 and Fig. 7.

**2.1.2 Nanomaterial adsorbents.** Nanomaterials possess high reactivity and catalytic potential and offer a higher surface area to particle size ratio.[42,43] Nanomaterials are gaining more interest in wastewater treatment due to their superior mechanical, optical, magnetic, and electrical properties. Nanomaterials in different forms, such as nanoparticles, nanosheets, nanorods, nanofibers, nanospheres, nanoribbons, quantum dots, and others, are used in wastewater treatment. The agglomeration of nanomaterials in wastewater reduces their performance.[44] The questions are raised about the separation of nanomaterials from effluents and their effects on human health. A nickel ferrite nanoparticle functionalized with silica ($SiO_2$) and aminosilane (APTS) ($NiFe_2O_4$@$SiO_2$@APTS) attained the adsorption performance of 59 mg $g^{-1}$ and 97% in 15 min of equilibrium time. The amine groups created on the nanocomposite adsorbent by coating APTS helped in the adsorption of IBU and other adsorbates. The adsorbent can be impregnated on thin films or matrices for continuous removal of IBU and other pharmaceuticals from wastewater.[45] This adsorbent is superparamagnetic with almost zero coercivity and remanence and quick response with an external magnetic field, which makes it easily separable from the solution after the adsorption process, reducing the centrifugation and filtration cost. This adsorbent was tested on a low IBU concentration of 12 mg $L^{-1}$, which only shows its better performance at low IBU concentration. It should be tested on higher IBU concentrations for practical feasibility in real applications. Corn starch nanoparticles (CSNP) achieved a removal efficiency of 86.33%. The toxicity analysis conducted on zebra fish showed that the LC50 (96 h) increased from 209.50 mg $L^{-1}$ to 1435.82 mg $L^{-1}$ after biosorption of IBU from an aqueous solution.[46] This work decreased the toxicity of the water and increased the LC50 of the zebrafish, but its removal efficiency needs further improvements to reach above 90% through proper surface functionalization with suitable compounds. The functionalization of CNT with COOH, $MnO_2$, and $Fe_2O_3$ increased the surface area of the CNT from 14.7 $m^2\ g^{-1}$ to 114.2 $m^2\ g^{-1}$ (Table 3). The PZC of CNT-COOH/$MnO_2$/$Fe_2O_3$ was at pH 6.5, and it was a hydrophobic adsorbent with a hydrophobicity index of 0.864. CNT-$Fe_3O_4$-$MnO_2$ nanocomposite achieved an adsorption capacity of 103.093 mg $g^{-1}$ in aqueous solution and removal efficiencies of 3.6% and 9.3% in two simulated pharmaceutical wastewaters.[47] This adsorbent showed good adsorption performance in an aqueous solution, but its performance is poor in simulated pharmaceutical wastewater. A composite adsorbent of activated black clay/rice flour/magnetite nanoparticles (BC/RF/MNPs) achieved a $q_m$ of 59.2 mg $g^{-1}$.[48] The adsorption energy between the adsorbent and IBU ranged between 0.42–3.42 kJ $mol^{-1}$, indicating physical interactions between them. This work developed an economical and environmentally friendly adsorbent. However, its adsorption capacity is lower than most other adsorbents. Natural piezoelectric quartz coated with green zinc oxide nanoparticles (GZnO/PQz) achieved an IBU adsorption capacity of 145.6 mg $g^{-1}$.[49] The increase in

Table 2 Adsorption performance of various adsorbents for the removal of Ibuprofen from wastewater

| Adsorbent | Performance | | Optimum parameters | | | | Ref. |
|---|---|---|---|---|---|---|---|
| | Adsorption capacity (mg $g^{-1}$) | $R$ (%) | pH | Dose (g $L^{-1}$) | $C$ (mg $L^{-1}$) | $t_{eq}$ (h) | |
| **Activated carbons** | | | | | | | |
| Carbon nanospheres (CNS) | 356.89 | — | 6 | 0.8 | — | 1.66 | 38 |
| Waste coffee-derived activated carbon (WAC) | 350 | — | 6.87 | 1 | — | 0.25 | 87 |
| Ethylamine-modified hydrophobic activated carbon (HAC-EA) | 35.21 | — | 7 | — | — | 10 | 23 |
| $TiO_2$ NPs modified groundnut shell activated carbon ($TiO_2$ NPs-GNSAC) | 55.56 | 81.78 | — | 0.5 | — | 0.83 | 36 |
| Biomass-derived activated carbon | 96.28 | — | 3 | 0.75 | — | — | 88 |
| *Nauclea diderrichii* biomass-derived activated carbon (NDAC) | 43.66 | — | 6 | 0.5 | — | 1 | 31 |
| *Erythrina speciosa* activated carbon (Ery-AC) | 98.11 | — | 3 | 0.75 | — | 1.66 | 39 |
| Reduced graphene oxide/activated carbon composite (RGO/AC1) | 85.57 | — | 2 | 0.4 | — | 1.667 | 89 |
| *Albizia lebbeck* seed pods activated carbon (MSAC) | 0.220 | — | 7.82 | 0.33 | 0.0764 | — | 90 |
| **Nanomaterials** | | | | | | | |
| $NiFe_2O_4$@$SiO_2$@APTS | 59 | 97 | 7 | — | 12 | 0.25 | 45 |
| Corn starch nanoparticles (CSNP) | — | 86.33 | 2 | 0.33 | 10 | — | 46 |
| Silver nanoparticles modified Luffa (LF/AgNPs) | 71.3 | 92 | 5 | 2.5 | 200 | 1 | 50 |
| CNT-$Fe_3O_4$-$MnO_2$ nanocomposite | 103.093 | — | 2 | 1 | 40 | 0.33 | 47 |
| Hemp seeds nanocomposite (HS-MnO/CuO) | 26.50 | | 8 | 0.4 | 100 | 0.5 | 91 |
| $TiO_2$/$Fe_2O_3$/chitosan nanocomposite | 166.667 | 95.2 | 7.3 | 0.05 | — | — | 92 |
| Hydrophobic deep eutectic solvents functionalized magnetic iron oxide nanoparticles ($Fe_3O_4$@HDES-2) | 23.6 | — | 3 | 4 | — | 0.333 | 51 |
| Zn-Decorated S, P, B coped $C_2N$ (Zn-SPB@ $C_2N$) nanosheet | — | 98 | 7 | 0.2 | 59 | — | 52 |
| Organo-silica nanosheets ($G_{16\text{-}2\text{-}16}$-SiNSs) | 64.19 | — | 4 | — | — | 0.083 | 93 |
| **Metal–organic framework (MOF)** | | | | | | | |
| Zirconium-based metal–organic framework (Zr-MOF) | 384.69 | — | — | 10 | — | 1.66 | 55 |
| Zirconium-based metal–organic framework modified with tryptophane (Zr-MOF-$NH_2$) | 371.34 | — | — | | — | — | |
| Magnetic carboxylic multiwalled carbon nanotube metal–organic framework (MCNTs-UiO-66-$NH_2$) | 143 | — | 1–10 | 1 | — | 2 | 58 |
| Cu-Doped Mil-101(Fe) | 497.3 | — | — | 0.2 | — | — | 57 |
| **Biochar** | | | | | | | |
| Iron and acid-modified date palm biochar (DPAI) | 72.2 | — | 2 | — | 150 | 20 | 62 |
| Recycled textile steam-activated biochar (RT-SABC) | 54 | 50 | — | — | — | 120 | 63 |
| Walnut shell-activated biochar (WSAB) | 69.7 | 80 | 4 | 1 | 50 | — | 64 |
| Plane tree leaf-derived biochar (P-BC) | 10.41 | 96.34 | 2 | 1 | 2 | 24 | 94 |
| Pinewood biochar | 10.74 | — | 3 | — | — | — | 61 |
| **Zeolites, cellulose, organoclays, chitosan, polymers, and other adsorbents** | | | | | | | |
| Acid-treated maize cob (AT-MC) | 36.81 | — | 6 | 6 | 75 | 0.66 | 95 |
| Cationic surfactant cetyldimethyl benzyl ammonium chloride (HDBAC) modified montmorillonite (H-Mt-1.6) | 81.64 | — | 5 | | | 2 | 86 |
| Molecularly imprinted Fe(III) incorporated chitosan hydrogels (CS_Fe_MIP) | 41.69 | — | 5 | — | — | — | 74 |
| Biomass derived chitosan | 24.21 | — | — | 7.5 | — | — | 72 |
| Polyethyleneimine modified magnetic sugarcane bagasse cellulose film (P-SBC/$Fe_3O_4$ film) | 370.52 | 92.63 | 4 | 0.0125 | — | 8 | 69 |

Table 2 (*Contd.*)

| Adsorbent | Performance | | Optimum parameters | | | | Ref. |
|---|---|---|---|---|---|---|---|
| | Adsorption capacity (mg $g^{-1}$) | $R$ (%) | pH | Dose (g $L^{-1}$) | $C$ (mg $L^{-1}$) | $t_{eq}$ (h) | |
| Metal–organic framework functionalized with hydrochar (MIL-53(Al)@HC) | — | 98 | 5.4 | — | — | 2 | 96 |
| Amine-grafted pumice derived silica aerogel (AMPDSA) | 39.95 | 100 | 7 | 0.5 | 6.53 | 2.5 | 85 |
| Fly ash derived zeolite modified by β-cyclodextrin (NaX-CD) | 31.3 | — | — | 0.5 | — | 0.25 | 67 |
| Iron-incorporated pomegranate husk carbon (NPH) | 39.77 | — | 8 | | 100 | 1 | 97 |
| Graphene oxide nanoplatelets (GONPs) | 3.72 | — | 6 | 1 | 6 | 1 | 98 |
| Activated bean husk (BHAA) | 24.570 | — | 4.75 | — | — | 0.66 | 99 |
| Rape straw biomass $Fe_3O_4$ treated and β-CD embedded adsorbent (RSBCDF) | 48.29 | — | 6 | 2.5 | — | 1 | 100 |
| Al/Li double layered hydroxide/polyaniline/sisal fibers composite (SF/PANI/LDH) | 86.03 | — | 5 | — | 100 | 1.5 | 101 |
| Steam activated coconut shell (CPBC) | 9.69 | — | 2 | 2.66 | 30 | 18 | 102 |
| Chemically activated ($H_3PO_4$) coconut shell (CCBC) | 12.16 | — | 2 | 3.33 | 25 | 18 | |
| Cellulosic sisal-poly (ppy-Ani) | 19.45 | 88 | 5 | 1.5 | 30 | 1 | 103 |
| Green synthesized iron oxide ($Fe_2O_3$) | 19.43 | 81.89 | 5 | 0.3 | 40 | 0.666 | 104 |
| Chitosan modified waste tire crumb rubber | 70 | — | 6 | — | — | 1 | 73 |
| Rice husk ash (RHA) | 2.321 | — | 2 | 10 | — | 4 | 105 |
| Carboxymethylcellulose/polypyrrole (CMC/PPY) composite | 72.30 | 83.17 | 7 | — | 10 | — | 106 |
| Multi-template molecularly imprinted polymer (MIP) | 3.598 | — | 4.6 | 5 | — | 0.166 | 78 |
| Porous polymer monoliths (PMLE-E) | 10.6 | 86.9 | 8 | — | — | 6 | 77 |
| Geopolymer | 5.7 | | 2 | — | — | — | 107 |

temperature decreased the adsorption active sites and saturation adsorption capacity, and the best adsorption was observed at 25 °C. Silver nanoparticles modified Luffa (LF/AgNPs) achieved an adsorption capacity of 41.3 mg $g^{-1}$ and a removal efficiency of 82.6% for IBU from real pharmaceutical wastewater samples, which is lower than its adsorption performance in aqueous solution.[50] The removal efficiency of IBU (5–40 mg $L^{-1}$) onto hydrophobic deep eutectic solvents functionalized magnetic iron oxide nanoparticles ($Fe_3O_4$@HDES-2) in spiked water with the presence of diclofenac was lower than diclofenac due to the presence of two aromatic rings in the structure of diclofenac.[51] Various machine learning (ML) models, such as Artificial Neural Network (ANN), Linear Regression (LR), Decision Tree (DT), and Random Forest (RF), are used to predict the performance of adsorbents. A study predicted the adsorption of IBU using zinc-decorated S, P, B co-doped $C_2N$ (Zn-SPB@$C_2N$) nanosheet and found that the Mean Squared Error (MSE) was lowest for RF model (3.70) compared to CCD model (36.56), ANN (28.12), DT (10.12), and LR (8.68). A maximum removal of 98% was obtained by using the RF model at optimized conditions.[52]

The surface area, pore size, and pore volume of NMs ranged between 16.849 and 328 $m^2$ $g^{-1}$, 0.019 and 4.8 nm, and 0.006 and 0.62 $cm^3$ $g^{-1}$, as shown in Table 3. In nano-sorbents, the adsorption capacities ranged between 23.6-166.667 mg $g^{-1}$. $TiO_2$/$Fe_2O_3$/chitosan nanocomposite and hydrophobic deep eutectic solvents functionalized magnetic iron oxide nanoparticles ($Fe_3O_4$@HDES-2) achieved the highest and lowest adsorption capacities, as shown in Table 3 and Fig. 7.

**2.1.3 Metal–organic framework (MOF).** MOFs are porous materials consisting of inorganic metal nodes and organic bridging ligands. MOFs possess a high porosity and high surface area, a high surface area to volume ratio, and tunable pore structure and surface chemistry.[53] Among the Zr-based MOFs prepared using different contents of commercial activated carbon and Benzoic Acid (BA), the UiO-67(Zr)-BA (10) attained the optimal performance at 213 mg $g^{-1}$.[54] This work developed an efficient adsorbent for IBU removal with an adsorption capacity three times higher than commercial activated carbon, which was due to a significant increase in surface area. The Zr-MOF-$NH_2$ obtained a $q_m$ of 371 mg $g^{-1}$. It exhibited a superior adsorption capability compared to bentonites, graphene oxide nanoplatelets (GONPs), organo silica nanosheets, and others.[55] This work developed an efficient adsorbent with good batch adsorption performance and recycling capability. However, dynamic adsorption and adsorption from real wastewater are necessary to further determine its real field application. The MIL-53 Raschig Rings (MIL-53 RR) prepared using alumina Raschig Rings achieved adsorption capacities ranging between 220 to 300 mg $g^{-1}$. The MIL-53-RR also showed good regeneration and resynthesis without affecting its performance.[56] This work developed an efficient and economical adsorbent that can be used for up to five cycles without losing its adsorption performance. A Cu-doped MIL-101 (Fe) adsorbent showed an adsorption capacity of 497.3 mg $g^{-1}$. Its adsorption capacity was unaffected by the addition of sodium chloride (NaCl) and natural organic matter (NOM). The lack of effect of

NaCl was due to the balance of competitive and salting out effects of NaCl, and the lack of effect of NOM was due to the presence of the required number of active sites for the adsorption of IBU and NOM or co-adsorption between IBU and NOM.[57] MCNTs-UiO-66-$NH_2$ showed good removal efficiency for IBU in simulated wastewater with removal efficiency above 99.99% at IBU concentration of 10 mg $L^{-1}$. However, at IBU concentration of 100 mg $L^{-1}$, the removal efficiencies decreased in the order of ionized water > tap water > lake water.[58] The effect of anions on the adsorption of IBU onto GGC-MOF200 was in the following order $SO_4^{2-}$ (78.68%) > $NO_3^-$ (81.12%) > $PO_4^{3-}$ (81.59%) > $HCO_3^-$ (85.87%) > $Cl^-$ (86.54%) while for actions the effect was in the order of $Ca^{2+}$ (72.86%) > $Cu^{2+}$ (75.81%) > $Mg^{2+}$ (76.95%) > $Zn^{2+}$ (81.73%) > $Pb^{2+}$ (85.56%).[67]

The surface area, pore size, and pore volume of MOFs ranged between 15.48 and 2900 $m^2$ $g^{-1}$, 2.093 and 14.4 nm, and 0.056 and 1.23 $cm^3$ $g^{-1}$, as shown in Table 3. The adsorption capacities of MOFs ranged between 143–497.3 mg $g^{-1}$. The Cu-doped MIL-101 (Fe) and MCNTs-UiO-66-$NH_2$ showed the highest and lowest adsorption capacities, respectively, as shown in Table 3 and Fig. 7.

**2.1.4 Biochar adsorbents.** Biochar is an economical carbon-rich material produced by the pyrolysis of biomass.[59] It has been reported that producing 1 ton of biochar costs 246 USD, while 1 ton of commercial activated carbon costs 1500 USD.[60] Various functional groups, such as ketone, carboxylic acids, ether, phenolic and aliphatic hydroxyl, and lactone groups, enhance their adsorption performance. The oxygen-containing functional groups can form hydrogen bonds with adsorbates in their protonated and deprotonated forms. The functional groups in biochar are not introduced from external agents, but they are oxygen of cellulose, hemicellulose, and lignin already present in biomass used to synthesize biochar. Their economic production and good performance make them alternative adsorbents to activated carbons.[61]

The adsorption capacity of iron and acid-modified date palm biochar (DPAI) was found to be 72.2 mg $g^{-1}$ (optimized using Box–Behnken Design (BBD) of RSM), superior to that of pine wood biochar, chemically activated *Cocos nucifera* shell biochar, and methanol-modified magnetic orange peel biochar, which is due to the increased adsorption sites and improved pore structure. DPAI had the most detrimental environmental effects of all the modified biochars, emitting 10.027 kg $CO_2$ eq $kg^{-1}$ and requiring 143.22 MJ $kg^{-1}$ in total energy consumption (CED) due to the modifications of biochar.[62] This work developed a modified adsorbent with enhanced adsorption performance, but its performance is lower than many other adsorbents, and its recycling efficiency is low. The high environmental impacts are the main drawbacks of this adsorbent. A steam-activated recycled textile biochar (RT-SABC) achieved an adsorption performance of 53.9 mg $g^{-1}$ and 50% at optimum conditions. Steam activation enhanced the surface area and micropore volume of the adsorbent. Its $pH_{PZC}$ was 10, indicating the abundance of carbonyl functional groups on its surface. The used adsorbent can be reused for energy production in gasification or syngas production.[63] This work showed that the microporous biochar had low adsorption capacity but

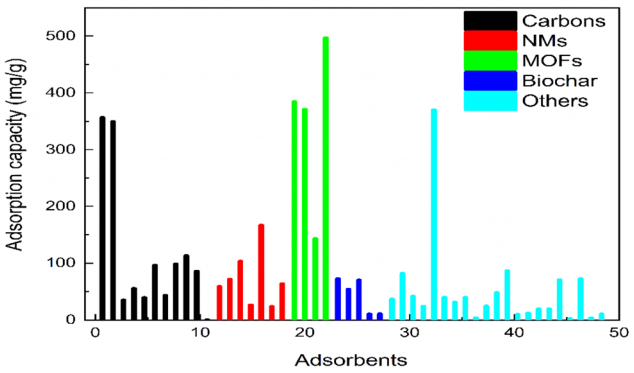


Fig. 7 A summary of the adsorption capacities of adsorbents.

fast kinetics. In contrast, steam-activated microporous and mesoporous biochar increased adsorption capacity but reduced the adsorption rate or kinetics. A walnut shell-activated biochar (WSAB) achieved a $q_m$ of 69.7 mg $g^{-1}$ with a maximum removal efficiency of 80%. With an estimated cost of USD 6.93 $kg^{-1}$ of adsorbent, this work produced a reasonably cheap and efficient adsorbent. This adsorbent also performed well in continuous adsorption, but its regeneration work should be conducted to further shed light on its commercial value.[64] A biochar derived from pepper steam achieved a maximum adsorption capacity of 569.6 mg $g^{-1}$ (experimental 18.23 mg $g^{-1}$).[65] This work shows that PS-biochar can remove IBU from wastewater; however, its experimental adsorption capacity is very low compared to most other adsorbents. Machine learning models of LR, DT, RF, Support Vector Machines (SVM), and k-Nearest Neighbor (k-NN) were used to predict the performance of biochar produced at 600–900 °C. Biochar produced at 900 °C achieved better performance than other biochar, and the RF algorithm predicted the best performance with 90.07% accuracy.[66]

The surface area, pore size, and pore volume of biochar ranged between 88.75 and 727.5 $m^2$ $g^{-1}$, 1.97 and 10.25 nm, and 0.059 and 0.57 $cm^3$ $g^{-1}$, as shown in Table 3. The adsorption capacity of biochar ranged between 10.41–72.2 mg $g^{-1}$. The DPAI and P-BC adsorbents achieved the highest and lowest adsorption capacities, respectively, as shown in Table 2 and Fig. 7.

**2.1.5 Zeolites, cellulose, organoclays, chitosan, polymers, and other adsorbents.** A β-cyclodextrin modified and fly ash-derived zeolite (NaX-CD) achieved a $q_m$ of 31.3 mg $g^{-1}$ within 15 min of equilibrium time.[67] NaX-CD is fast in removing IBU, but its adsorption capacity needs further improvement through the surface functionalization of zeolite with suitable compounds. The addition of octadecyldimethylbenzyl ammonium chloride (ODMBA), a cationic surfactant to bentonite, kaolin, and zeolite, resulted in the highest adsorption capacities of 147.4 mg $g^{-1}$, 7.54 mg $g^{-1}$, and 10.4 mg $g^{-1}$, respectively. These modified materials were then referred to as organo-bentonite (OB), organokaolin (OK), and organozeolite (OZ).[68] The highest adsorption of IBU onto OB adsorbent was due to the higher content of ODMBA. IBU's adsorption depended on the surfactant loading content, its configuration on the surface,

Table 3 Surface properties of adsorbents developed for IBU removal

| Adsorbent | Surface properties | | | Adsorption capacity ($mg\ g^{-1}$) | Ref. |
|---|---|---|---|---|---|
| | Surface area ($m^2\ g^{-1}$) | Pore size (nm) | Pore volume ($cm^3\ g^{-1}$) | | |
| **Activated carbons** | | | | | |
| *Erythrina speciosa* (Ery-AC) | 795 | 1.23 | 0.422 | 98.11 | 39 |
| $TiO_2$ NPs modified groundnut shell activated carbon ($TiO_2$ NPs-GNSAC) | 39.92 | 5.353 | 0.103 | 55.56 | 36 |
| *Nauclea diderrichii* biomass derived activated carbon (NDAC) | 33.2 | — | 0.037 | 43.66 | 31 |
| Ethylamine-modified hydrophobic activated carbon (HAC-EA) | 9.89 | 16.8 | 0.041 | 35.21 | 23 |
| Biomass-derived activated carbon | 795.1 | 1.232 | 0.422 | 96.28 | 88 |
| Ultrasound modified activated carbon (USAC) | 731.3 | 4.15 | 0.410 | 107.1 | 108 |
| Acid treated beverage sludge activated carbon (ABSAC) | 642 | 6.18 | 0.485 | 105.91 | 32 |
| Acid and thermally treated activated carbon cloth | 1946 | — | 0.80 | 491.9 | 109 |
| Mesoporous activated carbon (MAC) honeycomb | 358.20 | 2.46 | 0.21 | 16.730 | 110 |
| Nitrogen doped porous carbon (NPC-2) | 937 | 3.6 | 0.64 | 113 | 40 |
| Surface oxidized activated carbon ($AC700N_2$) | 809 | — | 0.55 | 160 | 111 |
| Magnetic nanoparticles incorporated on yeast-based activated carbon (NP-YC) | 644 | — | 0.41 | 51 | 35 |
| Carbon nanospheres (CNs) | 359 | — | 0.168 | 356.89 | 38 |
| Magnetic composite of nickel-iron oxide nanoparticles and activated carbon (NiAC) | 564 | 7.51 | 0.35 | 261.35 | 37 |
| Dried Alg/AC/CMC beads | 4.4 | 2.562 | 0.0017 | 34 | 41 |
| Hydrogel Alg/AC/CMC | 131.4 | 7.714 | 0.2027 | 39.6 | |
| Red mombin seeds (RMS) | 1508 | — | 0.778 | 69.88 | 33 |
| Corn cobs (CC) | 1280 | — | 0.661 | 88.03 | |
| External parts of mango seeds (MSEP) | 1279 | — | 0.700 | 52.60 | |
| **Nanomaterials** | | | | | |
| Hemp seeds nanocomposite (HS-MnO/CuO) | 21.55 | 0.019 | — | 26.50 | 91 |
| Organo-silica nanosheets ($G_{16\text{-}2\text{-}16}$-SiNSs) | 328 | 4.8 | 0.398 | 64.19 | 93 |
| Silver nanoparticles modified Luffa (LF/AgNPs) | 16.849 | — | 0.0065 | 71.3 | 50 |
| Natural piezoelectric quartz coated with green zinc oxide nanoparticles (GZnO/PQz) | 191.3 | — | 0.62 | 145.6 | 49 |
| **MOF** | | | | | |
| Zirconium-based metal–organic framework modified with tryptophane (Zr-MOF-$NH_2$) | 729.61 | — | 0.51 | 371.64 | 55 |
| Thermally activated gelatin–chitosan and amine-functionalized MOF aerogel (GGC-MOF200) | 819.6 | 2.093 | 0.430 | 5.963 | 112 |
| Cu-Doped Mil-101(Fe) | 15.48 | 14.4 | 0.056 | 497.3 | 57 |
| Zr-Based MOFs (UiO-67(Zr)-BA (10)) | 2900 | — | 1.23 | 213 | 54 |
| **Biochar** | | | | | |
| Iron and acid modified date palm biochar (DPAI) | 88.75 | 10.25 | 0.0591 | 72.2 | 62 |
| Recycled textile steam activated biochar (RT-SABC) | 710 | — | 0.3362 | 54 | 63 |
| Walnut shell-activated biochar (WSAB) | 686 | — | 0.57 | 69.7 | 64 |
| Biochar from pepper stem (PS-biochar) | 727.5 | 1.97 | 0.36 | 569.6 | 65 |
| **Zeolites, cellulose, organoclays, chitosan, polymers, and other adsorbents** | | | | | |
| Acid-treated maize cob (AT-MC) | 7.92 | 2.63 | 0.0213 | 36.81 | 95 |
| Cetyldimethyl benzyl ammonium chloride (HDBAC) modified montmorillonite (H-Mt-1.6) | 14.12 | 14.77 | 0.052 | 81.64 | 86 |

Table 3 (*Contd.*)

| Adsorbent | Surface properties | | | Adsorption capacity ($mg\ g^{-1}$) | Ref. |
|---|---|---|---|---|---|
| | Surface area ($m^2\ g^{-1}$) | Pore size (nm) | Pore volume ($cm^3\ g^{-1}$) | | |
| Molecularly imprinted Fe(III) incorporated chitosan hydrogels (CS_Fe_MIP) | 30.45 | 3.71 | 0.183 | 41.69 | 74 |
| Polyethyleneimine modified magnetic sugarcane bagasse cellulose film (P-SBC/$Fe_3O_4$ film) | 2.38 | 36.86 | 14.48 | 370.52 | 69 |
| Amine-grafted pumice derived silica (AMPDSA) | 407 | 5.45 | 1.05 | 39.95 | 85 |
| Fly ash derived zeolite modified by β-cyclodextrin (NaX-CD) | 68.69 | 3.875 | 0.041 | 31.3 | 67 |
| Biomass-derived chitosan | 6.57 | 87.3 | 0.0397 | 24.21 | 72 |
| Iron-incorporated pomegranate husk carbon (NPH) | 190 | 0.088 | — | 39.77 | 97 |
| Calcined spherical hydrochar (CSH) | 257.3 | 2.27 | 0.17 | 95.6 | 84 |
| $Ca^{2+}$(TAABB)Al | 208.39 | — | 0.275 | 17.54 | 113 |
| Rape straw biomass $Fe_3O_4$ treated and β-CD embedded adsorbent (RSBCDF) | 86.32 | 2.22 | — | 48.29 | 100 |
| Polydopamine imprinted polymers with fluorescent carbon dots (PIP-FCDs) | 184.09 | 3.63 | 0.094 | 209.8 | 76 |
| Acyl hydrazone covalent organic polymers (H-COP-3) | 8.558 | — | 0.069 | 242.775 | 79 |
| Versatile vermiculite modified by quinoline-based gemini surfactant (DHQU-Vt) | 2.53 | 23.51 | 0.015 | 240.69 | 83 |

and the physicochemical properties of IBU. This work developed modified adsorbents, and the OB adsorbent achieved the best adsorption performance. A polyethyleneimine-modified magnetic sugarcane bagasse cellulose film (P-SBC/$Fe_3O_4$ film) showed enhanced hydrophilicity due to PEI, which contains many hydrophilic functional groups. P-SBC/$Fe_3O_4$ film showed the adsorption performance of 370.52 mg $g^{-1}$ and 92.63%, respectively, at an equilibrium time of 8 h.[69] The higher adsorption performance was due to the increased hydrophilicity of the adsorbent. This work developed an efficient, economical, green, and magnetically separable adsorbent, but its adsorption equilibrium time is quite long. Two organoclays, a modified cationic octadecylamine natural montmorillonite ($C_{18}$-Mt) and a modified cationic octadecylamine synthetic mica ($C_{18}$-mica-4), achieved removal efficiencies of 99.9% (0.1–80 mg $L^{-1}$) and 99.99% to 67% (0.1–80 mg $L^{-1}$), respectively. $C_{18}$-Mt and $C_{18}$-mica-4 had the $pH_{PZC}$ at 6.5. The equilibrium was achieved faster for $C_{18}$-Mt than $C_{18}$-mica-4 (<5 min and 60 min).[70] In a separate investigation, IBU and its metabolites, namely 1-hydroxy ibuprofen (1-OH IBU), 2-hydroxy ibuprofen (2-OH IBU), and carboxy ibuprofen (CBX-IBU), were eliminated with adsorption capacities of 64, 20, 63, and 19 mg $g^{-1}$, respectively using $C_{18}$-Mt adsorbent.[71] The adsorption of IBU and its metabolites was lower in the combined solution due to the competition for active adsorption sites. This work developed an economical adsorbent for removing IBU and its metabolites from wastewater. Compared to other adsorbents, its adsorption capacity needs further improvement. The adsorption capacity of chitosan obtained from mud crab shells was 24.21 mg $g^{-1}$, surpassing most adsorbents derived from agricultural sources but falling short of activated carbons.[72] Its performance needs further improvement by increasing its surface properties and hydrogen bond acceptors by combining with suitable compounds or acid or alkaline treatment. The adsorption of IBU onto chitosan-modified waste crumb rubber in pond water, canal water, and tap water, with the presence of other pharmaceuticals such as diclofenac and naproxen, decreased compared to its performance in a single solution. In simulated wastewater, the adsorption of naproxen was higher compared to IBU and diclofenac due to the presence of secondary amine functional groups in its structure, which interact with chitosan and form hydrogen bonds.[73] The surface of molecularly imprinted Fe(III) incorporated chitosan hydrogels (CS_Fe_MIP) was porous and contained many pores and cavities, which can help in the adsorption of IBU. Its $pH_{PZC}$ was 7.85, indicating that it contains a positively charged surface for electrostatic interactions. When compared to chitosan without polymers, the adsorption performance of CS_Fe_MIP was significantly improved (79.41 mg $g^{-1}$). It also showed good adsorption performance in real water samples (34.06 mg $g^{-1}$ in tap water and 31.23 mg $g^{-1}$ in lake water). The adsorption capacity of CS_Fe_MIP decreased with the presence of naproxen in the solution (35.43–30.28 mg $g^{-1}$) due to the division of the active sites between the two adsorbates.[74] This work developed an efficient and recyclable adsorbent with good selectivity for IBU, but its performance in real wastewater samples is quite low.

The cross-linking of 2-hydroxypropyl-β-cyclodextrin polymers with poly(acrylic acid) obtained a $q_m$ of 87.5 mg $g^{-1}$ at an ideal pH of 5.[75] This work developed an effective modified polymer adsorbent with good recycling capability for up to ten cycles. A remarkable adsorption performance of 209.8 mg $g^{-1}$ and 99.9% was attained by polydopamine imprinted polymers with fluorescent carbon dots (PIP-FCDs). PIP-FCDs showed good detection sensitivity ($1.58 \times 10^{-5}$ μM) and high selectivity for IBU in the presence of other drugs such as ketoprofen, aspirin, levofloxacin, and norfloxacin. PIP-FCDs also showed good performance in real wastewater samples with recoveries of 97.65–98.81% for sewage water and 98.23–99.41% for tap water samples.[76] This work developed an efficient and economical bifunctional adsorbent (USD 1362.99 per ton) to detect and remove IBU from water. The removal efficiency of IBU onto porous polymer monoliths (PMLE-E) decreased in simulated waters and followed the following trend: distilled water (85.2%) > tap water (77.5%) > sea water (47.9%) > lake water (47%).[77] The adsorption of IBU onto Multi-template Molecularly Imprinted Polymer (MIP) ranged between 57% and 69% in river water and influent and effluent wastewaters.[78] The three-acyl hydrazone covalent organic polymers, namely H-COP-1, H-COP-2, and H-COP-3, demonstrated $q_m$ of 240.8 mg $g^{-1}$, 232.25 mg $g^{-1}$, and 242.775 mg $g^{-1}$, respectively, with an equilibrium adsorption time of 48 h.[79] The H-COP-3, which contains a higher number of acyl hydrazone bonds, showed better performance than H-COP-1 and H-COP-2 adsorbents. Though the adsorption capacity of this adsorbent is good, the higher adsorption time makes it an unfeasible adsorbent in real applications. Two adsorbents produced from cocoa shell biomass and functionalized with plasma and glycine had adsorption capacities ranging from 30.59 mg $g^{-1}$ to 38.95 mg $g^{-1}$. Surface functionalization enhanced the adsorbent's adsorption capability.[80] The adsorption performance of both adsorbents improved compared to the raw biomass. The adsorption performance of these adsorbents needs further improvement to compete with other adsorbents. The functionalizing materials can be changed with other suitable materials to further enhance the adsorption energy and density of active adsorption sites. A maize cob treated with a base (BMC) demonstrated changes in morphology to a net-like microstructure with more cavities. Its $pH_{PZC}$ was also increased from 5.35 to 6.75 due to the attachment of OH functional groups. BMC demonstrated an adsorption capacity and removal efficiency of 44.92 mg $g^{-1}$ and 91.07% at the best pH 8 and 80 min of equilibrium.[81] Treating maize cob with sodium hydroxide (NaOH) did not significantly increase surface area and adsorption performance compared to untreated maize cob (UMC). Therefore, other chemicals such as potassium hydroxide (KOH), phosphoric acid ($H_3PO_4$), and other suitable chemicals can be tested to further enhance surface area and adsorption performance. The magnetic anion exchange resins ND-1, ND-2, and ND-3 prepared using different contents of cyclohexanol exhibited a greater capacity for adsorbing IBU at a more rapid rate. This can be attributed to the larger pore width and volume, facilitating a more efficient internal diffusion process. The increase in cyclohexane content increased the surface area, pore size, and pore volume, which resulted in an increase in adsorption capacity and absorption rate due to the increase in internal diffusion of IBU. The adsorption of IBU was hindered by chloride and sulfate ions due to their competition for the active ion exchange sites. At 1 mmol $g^{-1}$ $L^{-1}$ of chloride and sulfate ions, the equilibrium adsorption capacities of ND-1, ND-2, and ND-3 were reduced by 63.5%, 56.9%, 48.8%, and 93%, 91.9%, 91.8%, respectively, showing a higher effect of sulfate due to its higher negative charge.[82] Although this study shared valuable information about the adsorption mechanism of IBU onto magnetic anion resins, the adsorption capacities are very low compared to other adsorbents, which need further improvements using any other suitable porogen agents. Versatile vermiculite modified by quinoline-based gemini surfactant (DHQU-Vt) showed a fluffy and rough surface, which will be helpful in the adsorption of IBU.[83] The modification of Na-VT by DHQU surfactant increased hydrophobicity, interlayer spacing, and decreased surface area and total pore volume. DHQU-Vt achieved a $q_m$ of 240.69 mg $g^{-1}$.[83] This work developed an efficient adsorbent for IBU removal, but further study on its continuous adsorption performance and IBU adsorption from real wastewater will shed light on its real-world applications. A calcined spherical hydrochar (CSH) showed the highest adsorption capacity of 95.6 mg $g^{-1}$ at 360 min of an equilibrium time.[84] This work developed an effective adsorbent for IBU removal, but its adsorption capacity needs further improvement, and the equilibrium time needs further reduction to compete with other adsorbents. An aerogel of AMPDSA achieved an adsorption capacity of 39.95 mg $g^{-1}$ at optimal parameters optimized using Central Composite Design (CCD) of RSM.[85] The amine-grafted pumice-derived silica aerogel (AMPDSA) exhibited uniform, amorphous, and spherical particles. These particles contained silica and had a distinct pearl-like structure. Amine grafting of PDSA decreased surface area by 37%, pore volume by 63%, and pore diameter by 41% due to the filling of the pores of aerogel with 3-aminopropyltriethoxysilane (APTES) molecules.[85] AMPDSA showed good adsorption capacity and 100% removal efficiency at optimum conditions, but the IBU concentration used was 2–10 mg $L^{-1}$. Its testing on higher IBU concentrations would further shed light on its performance. The montmorillonite adsorbent modified with Cetyl Dimethyl Benzyl Ammonium Chloride (HDBAC) with different dosages (0.8CEC–1.8CEC (cation exchange capacity)) showed that the H-Mt-16 ($q_e$ – 81.64 mg $g^{-1}$ and 13.14 mg $g^{-1}$ for H-Mt-16 and Ca-Mt, respectively) performed better than other adsorbents due to higher layer spacing of Ca-Mt-16 (3.31 nm) at this HDBAC loading.[86] The adsorption capacity of H-Mt-16 is better than many adsorbents, but it is lower than most adsorbents and needs further improvements using other suitable modifiers.

The adsorption performance of adsorbents is shown in Table 2 and Fig. 7, and the surface properties of adsorbents are shown in Table 3. The surface area ranges from 2.38 to 2900 $m^2$ $g^{-1}$, pore sizes from 0.0195 to 87.3 nm, and pore volumes from 0.006 to 14.48 $cm^3$ $g^{-1}$. The adsorbents exhibited adsorption capabilities ranging from 0.220 mg $g^{-1}$ to 497.3 mg $g^{-1}$. The removal efficiencies range between 50% to 100%. The adsorbents used to remove IBU were microporous and mesoporous. There seems to be no increasing or decreasing trend between the surface

properties and the adsorption capacity of adsorbents due to the involvement of many types of adsorption forces during the adsorption of IBU. The adsorbents consisted of acidic and basic functional groups, which helped in the adsorption of IBU. Adsorbents also showed porous structure and the presence of cavities and holes in their structures, which helped in the adsorption of IBU. Cu-doped Mil-101-(Fe) achieved the best experimental adsorption capacity of 497.3 mg $g^{-1}$. The optimum pH ranged between 1 to 10, the dosage between 0.0125 and 10 g $L^{-1}$, the IBU concentration between 0.0764 and 200 mg $L^{-1}$, and the equilibrium time between 0.083 and 120 h. The PS-biochar, Cu-doped Mil-1010 (Fe), Zr-MOF, Zr-MOF-$NH_2$, P-SBC/$Fe_3O_4$ film, and CNs exhibited adsorption capabilities over 300 mg $g^{-1}$. CNT-$Fe_2O_3$-$MnO_2$, $TiO_2$/$Fe_2O_3$-$MnO_2$, $TiO_2$/$Fe_2O_3$/chitosan nanocomposite, and MCNTs-Ui-66-$NH_2$ all had adsorption capacities greater than 100 mg $g^{-1}$, while for all other adsorbents, it was below 100 mg $g^{-1}$. More work has been reported on carbon; however, MOFs performed better than carbon, which shows that they have a higher capability to adsorb IBU, so more work should be conducted on developing efficient MOFs. Although the zeta potential of adsorbents has been the subject of relatively few investigations, it is an important parameter for understanding the adsorbent–adsorbate interactions. The zeta potential of newly developed adsorbents must be determined. Overall, the adsorbents effectively eliminated IBU from wastewater, and the modifications enhanced the adsorption performance compared to unmodified adsorbents.

### 2.2 Adsorption kinetics, isotherms, thermodynamics, and adsorption mechanism

The adsorption mechanism helps in understanding the adsorption process and designing new adsorbents. The adsorption mechanism of IBU was studied using kinetics, isotherms, thermodynamics, and simulation techniques. The pseudo-first order, pseudo-second order, and intraparticle diffusion models are commonly used kinetics models. The pseudo-second-order model was followed by most of the studies,[23,31,62] indicating IBU adsorption as a chemisorption process, while only a few studies followed other models.[63] The Freundlich, Langmuir, and Temkin isotherm models are commonly used in IBU adsorption studies. Most of the studies followed the Langmuir model, while a few followed other models, indicating the formation of a monolayer of IBU onto the surface of adsorbents.[23,31,62] Adsorption thermodynamics is studied to determine the Gibbs free energy ($\Delta G$), enthalpy ($\Delta H$), and entropy ($\Delta S$), and it helps in understanding the nature and type of adsorption. Most of the studies described adsorption of IBU as an endothermic process,[39,98,99] while some described it as an exothermic process.[31,83] The adsorption is physisorption if $\Delta H$ <40 kJ $mol^{-1}$ and chemisorption if $\Delta H$ is higher than 40 kJ $mol^{-1}$. Most studies described the adsorption of IBU as a physisorption process,[23,55,72,77,103,109] while some described it as a chemisorption process.[58,99,110] Most IBU adsorption studies showed negative values of $\Delta G$, indicating the spontaneity of the adsorption process, while the positive values of entropy showed

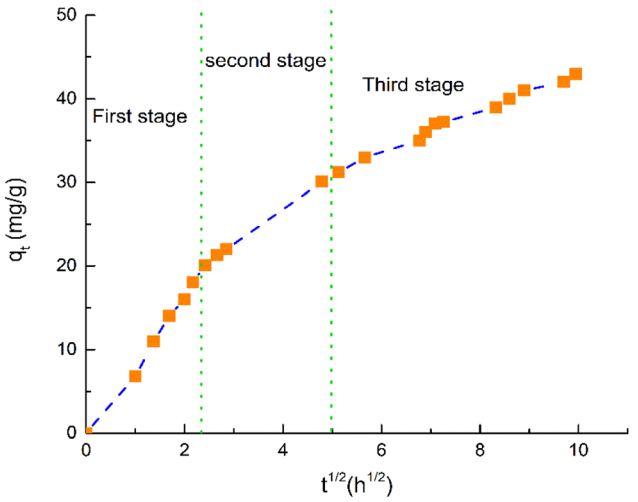


Fig. 8 Intraparticle diffusion model kinetics of IBU onto RT-SABC (redrawn).[63]

an increase in the entropy during the interaction between IBU and adsorbents.

The adsorption of IBU onto steam-activated recycled textile biochar (RT-SABC) involved ketone, amide, ester, aldehyde, carboxylic acid, aromatic ring groups, and ketones. The intraparticle diffusion kinetics model showed three adsorption phases, as shown in Fig. 8.[63] The first phase was quick and occurred on the external surface of the adsorbent for a duration of up to 7 h. The second stage took place on the inner surface of the adsorbent for 25 h. The third stage was the equilibrium stage, during which the adsorbate moved from macro- and mesopores to micropores. The graph skipped the origin, indicating that the rate-determining mechanism was not controlled by intraparticle diffusion. The IBU adsorbed onto AT-MC through electrostatic interactions, π–π interactions, H-bonding, Yoshida H-bonding, hydrophobic interactions, and π-interactions.[95] The adsorption of IBU onto iron-incorporated pomegranate husk carbon (NPH) occurred through π–π interactions, electrostatic interactions, Yoshida interactions, and hydrogen bonding.[97] The adsorption of IBU onto magnetically activated waste-activated coffee residue biochar (MACB) occurred through hydrogen bonding, π–π EDA interaction, and electrostatic interactions.[114] The IBU adsorbed onto scandium-modified oxo-triaryl methyl (Sc@oxTAM) through covalent interactions between Sc and oxygen (C=O) in the IBU, while onto other TM@oxTAM (Ti, V, Cr, and Mn) through covalent and electrostatic interactions.[115] The IBU adsorbed onto Zn-SPB@C2N by the formation of covalent bonds.[116]

The IBU adsorption mechanism onto activated carbon derived from tree pod biomass, determined using a double-layer model (DLM), is shown in Fig. 9. The IBU was adsorbed by forming two layers on the adsorbent. The first layer was formed through π–π interactions, hydrogen bonding, or π–anion interactions at a higher pH. The hydrogen bonding and π–π stacking were involved in forming the second layer. The first layer was deposited directly onto the adsorbent surface,

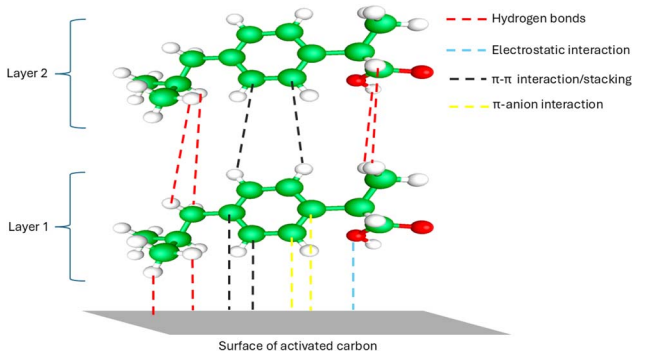


Fig. 9 Adsorption mechanism of IBU onto activated carbon (redrawn).[88]

whereas the subsequent layer was produced on top of the pre-existing layer on the adsorbent surface.[88] The IBU adsorbed onto biomass-derived chitosan through dipole–dipole and hydrogen bonding interactions. Amine and hydroxyl groups of chitosan were the H donors, while oxygen atoms of the carbonyl groups and heterocyclic ring were the H acceptors.[72] The adsorption of IBU onto PCDM-1000 occurred by hydrogen bonding through phenolic groups with PCDM and IBU as the hydrogen bond donors and acceptors, respectively. The hydrophobic and π–π interactions also participated in the adsorption.[34] The adsorption of IBU onto ultrasound-modified activated carbon (USAC) also occurred through donor–acceptor interactions.[108] The IBU adsorbed onto cocoa shell biomass-derived and plasma and glycine functionalized adsorbents through physical forces with adsorption energy in the range of 1.46–3.25 kJ $mol^{-1}$. The adsorption was controlled by the density of adsorption sites and the adsorption energy.[80] The IBU adsorbed onto CS_Fe_MIP monolith through interactions between chitosan functional groups, imprinted cavities, and iron hydroxide with IBU molecules. The electrostatic interactions between hydrogel and IBU, as well as the hydrogen bonding between the amine and hydroxyl group on chitosan and IBU, facilitated the adsorption.[74] The adsorption of IBU onto zeolite-sepiolite nanoheterostructures (Zeo-Sep) and modified organo-sepiolite (O-Sep) occurred through the formation of two layers. It occurred through horizontal and non-horizontal orientations, which depended on the temperature. The adsorption of IBU onto both adsorbents was a multimolecular and multi-docking process. The interactions between IBU/Zeo-Sep, IBU/O-Sep, and IBU/IBU displayed that it was a physisorption process.[117] The IBU adsorbed onto the P-SBC/$Fe_3O_4$ film through a multilayer process, primarily occurring by electrostatic interactions between the main amine of the P-SBC/$Fe_3O_4$ film and the carboxyl groups of IBU. Other interactions of van der Waals forces and hydrogen bonding were also involved in the absorption. An average of three to four active adsorbent sites shared one molecule of IBU.[69]

The adsorption of IBU onto DHQU-Vt adsorbent occurred through π–π stacking, π–π interactions, XH–π interactions, partition process, and electrostatic interactions. The density functional theory (DFT) simulations revealed that the intraparticle diffusion effect directly affected the molecular flexibility of the adsorbate, π–π stacking between isolated aromatic rings was stronger than between parallelly connected aromatic rings, and quinoline interactions like CH–π stacking, NH–π, and π–π interactions were weaker than electrostatic interactions/intraparticle diffusion.[83] The IBU adsorbed onto two MOFs,-UiO-66 and UiO-66-$NH_2$, through four interactions of hydrogen bonding, π–π EDA interactions, anion-π interactions, and Lewis acid/base complexing (LAB). The binding energies of these interactions decreased in the following order: π–π > hydrogen bonding > LAB > anion–π. The aggregation occurred at pH < pHpzc, and repulsion occurred at pH > pHpzc.[118] The adsorption of IBU onto activated carbon depended on the degree of dissociation of IBU. The changes in pH and temperature dissociated IBU (ionized[$A^-$] and non-ionized). At lower pH and higher temperatures, dissociation decreased, increasing adsorption capacity. Dissociation was high at pH > pHpzc, which caused repulsion between positively charged activated carbon species and negatively charged IBU species, and decreased the adsorption capacity.[119] The adsorption of IBU onto plasma-modified biomass occurred through the formation of two layers. The adsorption temperature determined the production of dimers and trimers in the solution. The adsorption occurred on inclined positions on the biomass surface, and thermal agitation and steric hindrance could affect the adsorption process.[120]

The IBU adsorbed onto different adsorbents through a variety of interactions, such as electrostatic interactions, π–π interactions, pore filling, pore diffusion, π–π EDA interactions, hydrogen bonding, and Yoshida interactions. The DFT has been used for determining the adsorption mechanism. However, molecular dynamics simulations can also be used in the future to determine the adsorption mechanism of IBU.

### 2.3 Regeneration and recycling

The regeneration of the adsorbent makes it economical and increases its commercial value. The IBU adsorbed adsorbents were regenerated using chemical and physical methods, as shown in Table 4. The PCDM-1000 was regenerated by washing with acetone and can be used for up to three consecutive cycles without any significant loss in activity.[34] GONPs showed no significant decrease in IBU removal efficiency up to eight regeneration cycles, while slightly decreased from 97.18% to 95.91% in the last two cycles ($9^{th}$ and $10^{th}$).[98] The BHHA adsorbent regenerated using HCl (0.2 M) showed an increase of removal efficiency from 88.75% ($1^{st}$ cycle) to 94.68% in four cycles.[99] The NP-YC can be reused consecutively for several cycles without desorption of IBU. The adsorption capacity declined gradually throughout eight cycles when the IBU concentration was 15 mg $L^{-1}$. However, it abruptly increased with increasing IBU concentration to 60 mg $L^{-1}$ in the ninth cycle. Subsequently, the adsorption capacity further decreased with increasing IBU concentration to 90 mg $L^{-1}$.[35] In the ninth cycle, the adsorption capacity was enhanced by increasing the amount of IBU molecules. However, this capacity was later diminished when the adsorbent reached saturation. The Ery-AC achieved good adsorption performance after regeneration for seven cycles. The adsorption capacity started to decrease after

Table 4 Recycling ability of adsorbents

| Adsorbent | Regeneration method | Cycles | Drop in removal efficiency (%) | Ref. |
|---|---|---|---|---|
| Carbon nanospheres (CNs) | Deionized water (DW) | 6 | 16.91 | 38 |
| BC/RF/MNPs | Mixture of water and acetone | 4 | 13.62 | 48 |
| $NiFe_2O_4$@$SiO_2$@APTS | NaOH (0.01 M) | 4 | 5 | 45 |
| Pepper stem-derived biochar (PS-biochar) | NaOH (0.1 M) | 4 | 22.27 | 65 |
| CMC/PPY | NaOH (1 M) | 5 | 36 | 106 |
| BMC | HCl (0.2 M) | 5 | 6.4 | 81 |
| CNT-$Fe_3O_4$-$MnO_2$ nanocomposite | HCl (0.1 M) | 5 | 6.2 | 47 |
| CPBC | Methanol | 4 | 18.6 | 102 |
| CCBC | | | 19 | |
| Pinewood biochar | Methanol | 4 | | 61 |
| CS_Fe_MIP monolith | Methanol | 4 | 15 | 74 |
| GGC-MOF200 | Methanol | 5 | 28.9 | 67 |
| PMLE-E | Methanol | 8 | 22.1 | 77 |
| RSBCDF | Methanol/acetic acid | 4 | 24.56 | 100 |
| DPAI | Oven (150 °C for 2 h) | 2 | 23.7 | 62 |
| NaX-CD | Ethanol | 5 | 77 | 67 |
| P-BC | Ethanol | 5 | 25.7 | 94 |
| LF/AgNPs | — | 4 | 10.8 | 50 |
| Cellulosic sisal-poly (ppy-Ani) | — | 4 | 16.7 | 103 |
| Zr-MOF-$NH_2$ | — | 5 | 16.8 | 55 |
| MCNTs-UiO-66-$NH_2$ | $NaHCO_3$ | 5 | | 58 |
| $Fe_3O_4$@HDES-2 | Acetonitrile | 5 | 5.8 | 51 |

seven cycles.[39] NPC-2 does not drop its adsorption capacity significantly up to four cycles.[40] Versatile vermiculite modified by quinoline-based gemini surfactant (DHQU-Vt) showed a good adsorption capacity up to three regeneration cycles, with a decrease of 8.13 mg $g^{-1}$ in adsorption capacity.[83] A Cu-doped Mil-101(Fe) maintained good removal efficiency for up to five regeneration cycles.[57] The UiO-67(Zr)-BA (10) can be utilized for a maximum of four cycles with a negligible decline in its adsorption capability.[54] Alg/AC/CMC retained an adsorption capacity equivalent to 93% of its initial adsorption capacity after ten regeneration cycles with a desorption efficiency above 80%.[41] The P-SBC/$Fe_3O_4$ film showed a very good recycling capability with 96% removal efficiency after 17 regeneration cycles.[69]

The recycling results of adsorbents are shown in Table 4. The drop in removal efficiency was determined based on the initial and final removal efficiencies. The removal efficiency after 1st regeneration was used where the initial removal efficiency was not given. It can be noticed that some adsorbents can be recycled up to 4 or 5 cycles. The regeneration of adsorbents with their drop in removal efficiency above 10% should be improved to make them more feasible. The regeneration and recycling of only a few adsorbents were conducted, and it is recommended that the regeneration and recycling of newly developed adsorbents be conducted to know more about their commercial feasibility. Future studies should focus on efficient, sustainable, green, and economical regeneration methods for the regeneration of adsorbents to avoid further pollution of the environment.

### 2.4 Continuous adsorption of ibuprofen (IBU)

The adsorption performance of adsorbents in continuous columns is especially important for their commercial feasibility. The RT-SABC attained a $q_m$ of 40 mg $g^{-1}$ when the bed height in the fixed-bed column was set at 30 cm. Upon increasing the bed height from 10 to 30 cm, the volume of effluent treated increased from 0.6 to 6.4 L at the breakthrough point, which occurred between 41.7 and 476.7 h, while the adsorption capacity increased from 22.09 to 39.81 mg $g^{-1}$.[63] The $Ca^{2+}$(TAABB)Al obtained an adsorption performance of 17.54 mg $g^{-1}$ and 97.48% at the best IBU concentration of 20 mg $L^{-1}$, bed height of 20 cm, and flow rate of 2 mL $min^{-1}$. The adsorbent displayed good IBU adsorption performance up to five regeneration cycles.[113] An SF/PANI/LDH composite demonstrated that increasing IBU concentration from 40 to 80 mg $L^{-1}$ and flow rate from 4 to 8 mL $min^{-1}$ decreased the adsorbate's service volume in a small fixed-bed column.[101] A walnut shell-activated biochar (WSAB) achieved a maximum adsorption capacity of 30.1 mg $g^{-1}$.[64]

It can be noticed that only a few studies have determined adsorbent performance in continuous mode using fixed-bed columns. It is impossible to evaluate the commercial feasibility of the adsorbent without its performance evaluation in the continuous mode. More research is needed to evaluate the commercial feasibility of adsorbents by focusing on refining the parameters and optimizing the regeneration process in continuous mode. Other continuous adsorption systems, such as moving beds, fluidized beds, and pulsed beds, should also be used to test the performance of adsorbents due to their widespread use in industries.

## 3. Future perspectives and challenges in the removal of IBU using adsorbents

Several adsorbents have been designed to remove IBU from wastewater, each with different levels of effectiveness. However, certain issues still need to be addressed in future studies.

The adsorption performances of *Nauclea diderrichii* biomass-derived activated carbon (NDAC), porous carbon derived from MOF (zeolitic-imidazolate framework-8 (ZIF-8)) (PCDMs), ethylamine-modified hydrophobic activated carbon (HAC-EA), magnetic nanoparticles incorporated on yeast-based activated carbon (NP-YC), iron and acid-modified date palm biochar (DPAI), β-cyclodextrin modified and fly ash-derived zeolite (NaX-CD), modified cationic octadecylamine natural montmorillonite ($C_{18}$-Mt), chitosan obtained from mud crab shells, two adsorbents produced from cocoa shell biomass and functionalized with plasma and glycine, maize cob treated with a base (BMC), calcined spherical hydrochar (CSH), and H-Mt-16 needs further improvement. Carbon nanospheres (CNs) only showed good adsorption in synthetic wastewater, while their performance in real wastewater needs further improvement. The removal efficiency of *Erythrina speciosa* activated carbon (Ery-AC) needs further enhancement at higher IBU concentrations. The adsorption performance of CNT-$Fe_3O_4$-$MnO_2$ nanocomposite needs improvement in simulated pharmaceutical wastewater. The adsorption performance of molecularly imprinted Fe(III) incorporated chitosan hydrogels (CS_Fe_MIP) is quite low and needs further enhancement. The equilibrium time of acyl hydrazone covalent organic polymers (H-COP-3) is quite high, which needs to be reduced. Generally, the adsorption performance of adsorbents can be increased by increasing the porosity, surface area, and number of active adsorption sites on the surface of the adsorbent by functionalization with suitable compounds. The adsorption performance of PCDMs can be enhanced by improving their surface chemistry by increasing the content of phenolic groups through doping with some suitable materials. NaX-CD is fast in removing IBU, but its adsorption capacity needs further improvement through the surface functionalization of zeolite with suitable compounds. The performance of chitosan obtained from mud crab shells can be enhanced by increasing its surface properties and hydrogen bond acceptors by combining with suitable compounds or acid or alkaline treatment. The adsorption performance of adsorbents obtained from cocoa shell biomass and functionalized with plasma and glycine can be enhanced by functionalization with other suitable materials to further enhance the adsorption energy and density of active adsorption sites. The adsorption performance of maize cob treated with sodium hydroxide (NaOH) can be enhanced by treating it with other chemicals, such as potassium hydroxide (KOH) and phosphoric acid ($H_3PO_4$). The performance of magnetic anion exchange resins (ND-1, ND-2, and ND-3) can be enhanced using other suitable porogen agents instead of cyclohexane.

Most of the adsorbents were only tested for IBU removal in batch mode; the adsorbents must also be tested for continuous adsorption of IBU to get more insights about their commercial feasibility. More focus should be put on developing highly efficient, economical, green, and regeneratable adsorbents that can adsorb multiple drugs from wastewater. Mass transfer adsorption kinetics should be studied to better understand adsorption processes. Statistical and machine learning tools such as Response Surface Methodology (RSM) and Artificial Neural Networks (ANN), Linear Regression (LR), Decision Tree (DT), and Random Forest (RF), Support Vector Machines (SVM), and k-Nearest Neighbor (k-NN) have been used to optimize the adsorption parameters. Artificial intelligence technologies should be utilized in IBU removal from wastewater to anticipate the adsorption capacity of adsorbents. The disposal of IBU adsorbed adsorbents should also be studied. The World Health Organization (WHO) standards for IBU removal should be followed in IBU removal processes for universal environmental protection.

## 4. Conclusions

Various adsorbents such as activated carbons, nanomaterials, metal–organic frameworks, biochar, and others have been developed to remove IBU from wastewater. The adsorbents were mostly mesoporous and a few macro- and microporous, with a surface area of 2.38 to 2900 $m^2\ g^{-1}$. The porous structure, the presence of cavities, and acidic and basic functional groups supported the adsorption of IBU. The Cu-doped Mil-101(Fe) adsorbent achieved the highest adsorption capacity of 497.3 mg $g^{-1}$, and *Albizia lebbeck* seed pods activated carbon (MSAC) achieved the lowest adsorption capacity of 0.220 mg $g^{-1}$. More activated carbons have been developed than other types of adsorbents. More focus has been put on batch adsorption on model wastewater with kinetics, isotherms, and thermodynamic studies. The adsorption of IBU involved electrostatic interactions, π–π interactions, pore filling, pore diffusion, π–π EDA interactions, hydrogen bonding, and Yoshida interactions. Future studies should focus more on developing highly efficient, economical, green, and regeneratable adsorbents that can adsorb multiple drugs from wastewater, adsorption of IBU and other pharmaceuticals from real wastewaters, continuous adsorption of IBU and other pharmaceuticals, mass transfer adsorption kinetics for a detailed understanding of the adsorption process, artificial intelligence technologies for predicting the adsorption capacity of adsorbents and the removal efficiency of adsorbents, and the disposal of IBU adsorbed adsorbents.

## Data availability

No primary research results, software, or code have been included, and no new data were generated or analyzed as part of this review.

## Author contributions

Ahmer Ali Siyal writing – original draft. Radin Maya Saphira Radin Mohamed supervision. Faizan Ahmed writing – review and editing. Marlinda Abdul Malek writing – review and editing. Majed Alsubih visualization. Rashid Shamsuddin writing – review and editing. Sajid Hussain writing – review and editing. Sabariah Musa resources.

## Conflicts of interest

There are no conflicts to declare.

## Acknowledgements

The authors extend their appreciation to the Deanship of Research and Graduate Studies at King Khalid University Saudi Arabia for funding this work through the Large Research Project under grant number RGP2/67/46 and to the Ministry of Higher Education (MOHE) Malaysia through the Fundamental Research Grant Scheme (FRGS/1/2024/WAS02/UTHM/02/5).

## References

1 K. Fent, A. A. Weston and D. Caminada, *Aquat. Toxicol.*, 2006, **76**, 122–159.
2 C. Stamm, K. Räsänen, F. J. Burdon, F. Altermatt, J. Jokela, A. Joss, M. Ackermann and R. I. L. Eggen, in *Advances in Ecological Research*, ed. A. J. Dumbrell, R. L. Kordas and G. Woodward, Academic Press, 2016, vol. 55, pp. 183–223.
3 R. B. González-González, P. Sharma, S. P. Singh, J. H. P. Américo-Pinheiro, R. Parra-Saldívar, M. Bilal and H. M. N. Iqbal, *Sci. Total Environ.*, 2022, **821**, 153329.
4 Y. Zhang, S.-U. Geißen and C. Gal, *Chemosphere*, 2008, **73**, 1151–1161.
5 J. H. Al-Rifai, C. L. Gabelish and A. I. Schäfer, *Chemosphere*, 2007, **69**, 803–815.
6 T. A. Ternes, *Water Res.*, 1998, **32**, 3245–3260.
7 L. H. M. L. M. Santos, M. Gros, S. Rodriguez-Mozaz, C. Delerue-Matos, A. Pena, D. Barceló and M. C. B. S. M. Montenegro, *Sci. Total Environ.*, 2013, **461–462**, 302–316.
8 K. V. Thomas, C. Dye, M. Schlabach and K. H. Langford, *J. Environ. Monit.*, 2007, **9**, 1410–1418.
9 P. Verlicchi, M. Al Aukidy, A. Galletti, M. Petrovic and D. Barceló, *Sci. Total Environ.*, 2012, **430**, 109–118.
10 Y. Luo, W. Guo, H. H. Ngo, L. D. Nghiem, F. I. Hai, J. Zhang, S. Liang and X. C. Wang, *Sci. Total Environ.*, 2014, **473–474**, 619–641.
11 M. Al Sharabati, R. Abokwiek, A. Al-Othman, M. Tawalbeh, C. Karaman, Y. Orooji and F. Karimi, *Environ. Res.*, 2021, **202**, 111694.
12 K. Pazdro, M. Borecka, G. Siedlewicz, A. Biak-Bieliska and P. Stepnowski, *Curr. Anal. Chem.*, 2016, **12**, 202–226.
13 J. Sharma, M. Joshi, A. Bhatnagar, A. K. Chaurasia and S. Nigam, *Environ. Res.*, 2022, **215**, 114219.
14 E. Emmanuel, Y. Perrodin, G. Keck, J. M. Blanchard and P. Vermande, *J. Hazard. Mater.*, 2005, **117**, 1–11.
15 S. Bancos, M. P. Bernard, D. J. Topham and R. P. Phipps, *Cell. Immunol.*, 2009, **258**, 18–28.
16 S. Chopra and D. Kumar, *Heliyon*, 2020, **6**, e04087.
17 Y. Li, G. Zhu, W. J. Ng and S. K. Tan, *Sci. Total Environ.*, 2014, **468–469**, 908–932.
18 S. Álvarez-Torrellas, A. Rodríguez, G. Ovejero and J. García, *Chem. Eng. J.*, 2016, **283**, 936–947.
19 A. S. Mestre, J. Pires, J. M. F. Nogueira and A. P. Carvalho, *Carbon*, 2007, **45**, 1979–1988.
20 BASF, 2022.
21 M. Caban, A. Bialk-Bielinska, P. Stepnowski and J. Kumirska, *Curr. Anal. Chem.*, 2016, **12**, 249–257.
22 S. Chopra and D. J. H. Kumar, *Heliyon*, 2020, **6**, e04087.
23 S. N. F. Ali, E. I. El-Shafey, S. Al-Busafi and H. A. J. Al-Lawati, *J. Environ. Chem. Eng.*, 2019, **7**, 102860.
24 S. Show, P. Chakraborty, B. Karmakar and G. Halder, *Sci. Total Environ.*, 2021, **786**, 147327.
25 S. N. Oba, J. O. Ighalo, C. O. Aniagor and C. A. Igwegbe, *Sci. Total Environ.*, 2021, **780**, 146608.
26 F. Ahmad, *Heliyon*, 2023, **9**, e16449.
27 J.-l. Wu, Z.-h. Liu, Q.-g. Ma, L. Dai and Z. Dang, *Sci. Total Environ.*, 2023, **891**, 164600.
28 A. Ayati, B. Tanhaei, H. Beiki, P. Krivoshapkin, E. Krivoshapkina and C. Tracey, *Chemosphere*, 2023, **323**, 138241.
29 P. Madariaga-Segovia, S. Párraga and C. A. Villamar-Ayala, *Bioresour. Technol. Rep.*, 2023, **23**, 101564.
30 M. J. Ahmed, *J. Environ. Manage.*, 2017, **190**, 274–282.
31 M. O. Omorogie, J. O. Babalola, M. O. Ismaeel, J. D. McGettrick, T. M. Watson, D. M. Dawson, M. Carta and M. F. Kuehnel, *Adv. Powder Technol.*, 2021, **32**, 866–874.
32 A. F. M. Streit, G. C. Collazzo, S. P. Druzian, R. S. Verdi, E. L. Foletto, L. F. S. Oliveira and G. L. Dotto, *Chemosphere*, 2021, **262**, 128322.
33 L. Matějová, J. Bednárek, J. Tokarský, I. Koutník, B. Sokolová and G. J. F. Cruz, *Appl. Surf. Sci.*, 2022, **605**, 154607.
34 B. N. Bhadra, I. Ahmed, S. Kim and S. H. Jhung, *Chem. Eng. J.*, 2017, **314**, 50–58.
35 G. Labuto, A. P. Carvalho, A. S. Mestre, M. S. dos Santos, H. R. Modesto, T. D. Martins, S. G. Lemos, H. D. T. da Silva, E. N. V. M. Carrilho and W. A. Carvalho, *Sustain. Chem. Pharm.*, 2022, **28**, 100703.
36 I. A. Olowonyo, K. K. Salam, M. O. Aremu and A. Lateef, *Waste Manag. Bull.*, 2024, **1**, 217–233.
37 A. C. Fröhlich, E. L. Foletto and G. L. Dotto, *J. Clean. Prod.*, 2019, **229**, 828–837.
38 A. A. Alluhaybi, A. M. Hameed, M. T. Alotaibi, A. Alharbi and A. Shahat, *J. Mol. Liq.*, 2023, **383**, 122059.
39 D. S. P. Franco, D. Pinto, J. Georgin, M. S. Netto, E. L. Foletto, C. Manera, M. Godinho, L. F. O. Silva and G. L. Dotto, *J. Environ. Chem. Eng.*, 2022, **10**, 108070.
40 X. Lei, L. Huang, K. Liu, L. Ouyang, Q. Shuai and S. Hu, *J. Colloid Interface Sci.*, 2021, **604**, 823–831.
41 J. W. Lee, J. Han, Y.-K. Choi, S. Park and S. H. Lee, *Int. J. Biol. Macromol.*, 2023, **249**, 126053.
42 A. A. Basheer, *J. Mol. Liq.*, 2018, **261**, 583–593.
43 G. Z. Kyzas and K. A. Matis, *J. Mol. Liq.*, 2015, **203**, 159–168.
44 S. C. Endres, L. C. Ciacchi and L. Mädler, *J. Aerosol Sci.*, 2021, **153**, 105719.
45 S. Chandrashekar Kollarahithlu and R. M. Balakrishnan, *J. Clean. Prod.*, 2021, **294**, 126155.
46 V. Priyan and S. Narayanasamy, *Environ. Toxicol. Pharmacol.*, 2022, **94**, 103930.
47 I. Lung, M.-L. Soran, A. Stegarescu, O. Opris, S. Gutoiu, C. Leostean, M. D. Lazar, I. Kacso, T.-D. Silipas and A. S. Porav, *J. Hazard. Mater.*, 2021, **403**, 123528.
48 A. M. Badawy, A. A. Farghali, A. Bonilla-Petriciolet, M. K. Seliem, A. Q. Selim, M. A. Ali, M. Al-Dossari,

N. S. A. El-Gawaad, M. Mobarak, E. C. Lima and H. I. Bendary, *J. Taiwan Inst. Chem. Eng.*, 2023, **152**, 105177.
49 X. Yang, J. Wang, A. M. El-Sherbeeny, A. A. AlHammadi, W.-H. Park and M. R. Abukhadra, *Chem. Eng. J.*, 2022, **431**, 134312.
50 S. Joodaki and A. Mollahosseini, *Environ. Nanotechnol. Monit. Manag.*, 2023, **20**, 100823.
51 N. M. Hashim, M. Mohamad, N. N. S. N. M. Kamal, M. Y. Aziz, S. Mohamad, N. Yahaya and N. N. M. Zain, *J. Mol. Liq.*, 2023, **383**, 122082.
52 M. Khajavian and A. Haseli, *J. Ind. Eng. Chem.*, 2024, **137**, 583–592.
53 M. H. Manzoor, N. Naz, S. M. G. Naqvi, S. Ashraf, M. Z. Ashiq and F. Verpoort, *Appl. Mater. Today*, 2024, **40**, 102358.
54 M. M. H. Mondol, D. K. Yoo and S. H. Jhung, *J. Environ. Chem. Eng.*, 2022, **10**, 108560.
55 N. D. Alkhathami, N. A. Alamrani, A. Hameed, S. D. Al-Qahtani, R. Shah and N. M. El-Metwaly, *Polyhedron*, 2023, **235**, 116349.
56 T. Wu, N. Prasetya and K. Li, *J. Environ. Chem. Eng.*, 2022, **10**, 107432.
57 P. Xiong, H. Zhang, G. Li, C. Liao and G. Jiang, *Sci. Total Environ.*, 2021, **797**, 149179.
58 X. Zhang, C. Gao, R. Wang and R. Han, *J. Environ. Chem. Eng.*, 2023, **11**, 111090.
59 M. M. Hassan and C. M. Carr, *Chemosphere*, 2021, **265**, 129087.
60 M. Ahmad, A. U. Rajapaksha, J. E. Lim, M. Zhang, N. Bolan, D. Mohan, M. Vithanage, S. S. Lee and Y. S. Ok, *Chemosphere*, 2014, **99**, 19–33.
61 M. Essandoh, B. Kunwar, C. U. Pittman, D. Mohan and T. Mlsna, *Chem. Eng. J.*, 2015, **265**, 219–227.
62 J. F. Shaheen, J. O. Eniola and B. Sizirici, *Bioresour. Technol. Rep.*, 2024, **25**, 101696.
63 C. Rabbat, A. Pinna, Y. Andres, A. Villot and S. Awad, *J. Water Proc. Eng.*, 2023, **53**, 103830.
64 M. Patel, A. K. Chaubey, C. U. Pittman and D. Mohan, *Environ. Sci.:Adv.*, 2022, **1**, 530–545.
65 A. Naima, F. Ammar, O. Abdelkader, C. Rachid, H. Lynda, A. Syafiuddin and R. Boopathy, *Bioresour. Technol.*, 2022, **347**, 126685.
66 M. R. Islam, Q. Wang, S. Sharmin and C. E. Enyoh, *Water*, 2024, **16**, p. 3469.
67 L. Bandura, M. Białoszewska, S. Malinowski and W. Franus, *Appl. Surf. Sci.*, 2021, **562**, 150160.
68 M. Obradović, A. Daković, D. Smiljanić, M. Ožegović, M. Marković, G. E. Rottinghaus and J. Krstić, *Microporous Mesoporous Mater.*, 2022, **335**, 111795.
69 Y. Liu, Y.-S. Xiong, M.-X. Li, W. Li and K. Li, *Int. J. Biol. Macromol.*, 2024, **265**, 130969.
70 J. Martín, M. d. M. Orta, S. Medina-Carrasco, J. L. Santos, I. Aparicio and E. Alonso, *Appl. Clay Sci.*, 2019, **171**, 29–37.
71 J. L. Malvar, J. Martín, M. d. M. Orta, S. Medina-Carrasco, J. L. Santos, I. Aparicio and E. Alonso, *Appl. Clay Sci.*, 2020, **189**, 105529.
72 E. W. E. S. Shahrin, N. A. H. Narudin, N. N. M. Shahri, M. Nur, J.-W. Lim, M. R. Bilad, A. H. Mahadi, J. Hobley and A. Usman, *Emerging Contam.*, 2023, **9**, 100199.
73 W. Phasuphan, N. Praphairaksit and A. Imyim, *J. Mol. Liq.*, 2019, **294**, 111554.
74 M. Stachowiak, M. Cegłowski and J. Kurczewska, *Int. J. Biol. Macromol.*, 2023, **251**, 126356.
75 J. Wang and F. Yang, *Mater. Lett.*, 2021, **284**, 128882.
76 I. Mohiuddin, R. Singh and V. Kaur, *Int. J. Biol. Macromol.*, 2024, **269**, 131765.
77 M. Sözbir, E. B. Simsek, H. H. Mert, B. Kekevi, M. S. Mert and E. H. Mert, *Microporous Mesoporous Mater.*, 2023, **354**, 112509.
78 L. M. Madikizela and L. Chimuka, *J. Environ. Chem. Eng.*, 2016, **4**, 4029–4037.
79 H. Zhu, C. Ni, L. Zhou, Y. Chen and Y. Qin, *J. Environ. Chem. Eng.*, 2023, **11**, 109228.
80 H. A. Al-Yousef, B. M. Alotaibi, F. Aouaini, L. Sellaoui and A. Bonilla-Petriciolet, *J. Mol. Liq.*, 2021, **331**, 115697.
81 P. M. Thabede, N. A. H. Khumalo, P. N. Mahlambi, P. Nyamukamba and S. J. Modise, *S. Afr. J. Chem. Eng.*, 2023, **46**, 376–385.
82 J. Wang, H. Li, C. Shuang, A. Li, C. Wang and Y. Huang, *Microporous Mesoporous Mater.*, 2015, **210**, 94–100.
83 T. Shen, T. Han, Q. Zhao, F. Ding, S. Mao and M. Gao, *Chemosphere*, 2022, **295**, 133846.
84 S.-H. Yoo, S.-C. Lee, H.-Y. Jang and S.-B. Kim, *Chemosphere*, 2023, **311**, 137074.
85 A. Mohseni-Bandpei, A. Eslami, H. Kazemian, M. Zarrabi and T. J. Al-Musawi, *Environ. Technol. Innovat.*, 2020, **18**, 100642.
86 Y. Chu, Y. Dai, M. Xia, X. Xing, F. Wang, Y. Li and H. Gao, *Colloids Surf., A*, 2024, **681**, 132764.
87 T. Xing, Y. Wu, Q. Wang, A. Sadrnia, A. Behmaneshfar and E. N. Dragoi, *Environ. Res.*, 2023, **231**, 116223.
88 M. Bouzidi, L. Sellaoui, M. Mohamed, D. S. P. Franco, A. Erto and M. Badawi, *J. Mol. Liq.*, 2023, **376**, 121457.
89 P. Ndagijimana, X. Liu, Q. Xu, Z. Li, B. Pan and Y. Wang, *Sep. Purif. Technol.*, 2022, **299**, 121681.
90 N. Sivarajasekar, N. Mohanraj, S. Sivamani, J. Prakash Maran, I. Ganesh Moorthy and K. Balasubramani, *Mater. Today: Proc.*, 2018, **5**, 7264–7274.
91 B. R. Mphuthi, P. M. Thabede, M. E. Monapathi and N. D. Shooto, *Case Stud. Chem. Environ. Eng.*, 2023, **8**, 100436.
92 M. Rajamehala, A. M. Kumara Pandian, M. Rajasimman and B. Gopalakrishnan, *Environ. Res.*, 2023, **218**, 114984.
93 H. Zeng, M. Gao, T. Shen and F. Ding, *J. Taiwan Inst. Chem. Eng.*, 2018, **93**, 329–335.
94 X. Yang, X. Zhang, H. H. Ngo, W. Guo, J. Huo, Q. Du, Y. Zhang, C. Li and F. Yang, *J. Water Proc. Eng.*, 2022, **46**, 102627.
95 P. M. Thabede, *Case Stud. Chem. Environ. Eng.*, 2024, **9**, 100718.
96 J. M. Navia Mendoza, B. F. Rivadeneira Mendoza, J. Cevallos Mendoza, A. M. Balu, R. Luque, L. A. Zambrano Intriago and J. M. Rodríguez-Díaz, *Environ. Res.*, 2024, **240**, 117492.

97 N. D. Shooto, *Heliyon*, 2023, **9**, e20268.
98 P. Banerjee, P. Das, A. Zaman and P. Das, *Process Saf. Environ. Prot.*, 2016, **101**, 45–53.
99 O. S. Bello, O. C. Alao, T. C. Alagbada and A. M. Olatunde, *Sustain. Chem. Pharm.*, 2019, **13**, 100151.
100 G. Wu, Q. Liu, J. Wang, S. Xia, H. Wu, J. Zong, J. Han and W. Xing, *Ind. Crops Prod.*, 2021, **173**, 114150.
101 M. Negarestani, S. Reisi, M. Sohrabi, H. Shayesteh, H. Farimaniraad, A. Mollahosseini, M. Hosseinzadeh and S. Tavassoli, *J. Water Proc. Eng.*, 2024, **57**, 104657.
102 P. Chakraborty, S. Show, W. Ur Rahman and G. Halder, *Process Saf. Environ. Prot.*, 2019, **126**, 193–204.
103 A. Khadir, M. Motamedi, M. Negarestani, M. Sillanpää and M. Sasani, *Int. J. Biol. Macromol.*, 2020, **162**, 663–677.
104 A. Sherazi, G. Hussain, M. Anis and S. Aurangzeb, *Desalination Water Treat.*, 2024, **317**, 100151.
105 D. D. Andi Grefa, J. E. Guevara Sánchez, L. R. Bravo Sánchez, M. S. Pomares Alfonso and M. E. Villanueva Tagle, *Microchem. J.*, 2023, **195**, 109361.
106 V. P. V., N. Kumar, H. K. Rajendran, J. Ray and S. Narayanasamy, *Int. J. Biol. Macromol.*, 2022, **221**, 547–557.
107 R. Paparo, M. Di Serio, G. Roviello, C. Ferone, M. Trifuoggi, V. Russo and O. Tarallo, *Molecules*, 2024, **29**, 2210.
108 A. C. Fröhlich, R. Ocampo-Pérez, V. Diaz-Blancas, N. P. G. Salau and G. L. Dotto, *Chem. Eng. J.*, 2018, **341**, 65–74.
109 H. Guedidi, L. Reinert, Y. Soneda, N. Bellakhal and L. Duclaux, *Arab. J. Chem.*, 2017, **10**, S3584–S3594.
110 S. P. Dubey, A. D. Dwivedi, M. Sillanpää and K. Gopal, *Chem. Eng. J.*, 2010, **165**, 537–544.
111 H. Guedidi, L. Reinert, J.-M. Lévêque, Y. Soneda, N. Bellakhal and L. Duclaux, *Carbon*, 2013, **54**, 432–443.
112 M. Kim, L. K. Njaramba, Y. Yoon, M. Jang and C. M. Park, *Carbohydr. Polym.*, 2024, **324**, 121436.
113 S. Show, R. Sarkhel and G. Halder, *Sustain. Chem. Pharm.*, 2022, **27**, 100698.
114 J. Shin, J. Kwak, S. Kim, C. Son, Y.-G. Lee, S. Baek, Y. Park, K.-J. Chae, E. Yang and K. Chon, *J. Environ. Chem. Eng.*, 2022, **10**, 107914.
115 S. Kaviani, M. Khajavian, I. Piyanzina, O. V. Nedopekin and D. A. Tayurskii, *J. Mol. Graph. Model.*, 2024, **126**, 108647.
116 M. Khajavian, S. Kaviani, I. Piyanzina, D. A. Tayurskii and O. V. Nedopekin, *Colloids Surf., A*, 2024, **680**, 132702.
117 Z. Li, A. Gómez-Avilés, L. Sellaoui, J. Bedia, A. Bonilla-Petriciolet and C. Belver, *Chem. Eng. J.*, 2019, **371**, 868–875.
118 W. Sun, H. Li, H. Li, S. Li and X. Cao, *Chem. Eng. J.*, 2019, **360**, 645–653.
119 P. Iovino, S. Canzano, S. Capasso, A. Erto and D. Musmarra, *Chem. Eng. J.*, 2015, **277**, 360–367.
120 H. A. Al-Yousef, B. M. Alotaibi, M. M. Alanazi, F. Aouaini, L. Sellaoui and A. Bonilla-Petriciolet, *J. Environ. Chem. Eng.*, 2021, **9**, 104950.